Alexandria Engineering Journal (2023) 63, 233–252

HOSTED BY

Alexandria University

Alexandria Engineering Journal

www.elsevier.com/locate/aej
www.sciencedirect.com

Power correlations as complementary tools for generalised analysis and preliminary design of Stirling engines

Jesús-Ignacio Prieto *, **David García**

Gijón Polytechnic School of Engineering, University of Oviedo, Spain

Received 5 July 2021; revised 14 June 2022; accepted 31 July 2022
Available online 06 August 2022

KEYWORDS

Stirling engine;
Prototype analysis;
Preliminary design;
Dimensionless variables;
Maximum power condition;
Correlations

Abstract The use of dimensionless variables facilitates the generalised analysis of Stirling engines and provides tools for preliminary design, validation of simulation codes and feasibility studies of energy conversion systems. This article provides correlations to estimate the dimensionless values of maximum indicated and brake power, as well as their corresponding speeds. The concept of effective pressure allows power correlations to be related to gas circuit models and mechanical efficiency calculations. Previous correlations based on data from eight very different prototypes are revised using the criterion of minimising the relative root mean square errors (RRMSE) and sensitivity analysis to select influential variables. The application of previously established performance models provided additional data from the M102C and ST05G engines for validation purposes. The procedure also allows detecting inconsistent measurements. Data deviations seem acceptable for most operating points of the 10 analysed engines. The errors inherent to the procedure, as well as the number and quality of experimental data, determine the following average values of accuracy indicators: RRMSE = 3.20% for the dimensionless maximum indicated power, RRMSE = 6.35% for the dimensionless speed corresponding to the maximum indicated power, RRMSE = 6.39% for the dimensionless maximum brake power, and RRMSE = 10.93% for the dimensionless speed corresponding to the maximum brake power.

1. Introduction

Traditionally, it is argued that the Stirling engine is especially interesting for its relatively high efficiency, and it is indeed a fact that small Stirling engines have achieved brake efficiency values comparable to those of large Diesel engines. However, the multifuel capability of a Stirling engine, including renewable sources, is probably a greater advantage in the current context of energy saving and sustainability, as

* Corresponding author at: Edificio Departamental Este, c/Wifredo Ricart s/n, Gijón, España.
E-mail address: jprieto@uniovi.es (J.-I. Prieto).
Peer review under responsibility of Faculty of Engineering, Alexandria University.

https://doi.org/10.1016/j.aej.2022.07.061

Nomenclature

A_{wx}	wetted area of space ×, m^2
C_f	friction factor
L_R	regenerator length, m
M	mass of working fluid, kg
$\dot{m}_x$	mass flow rate at cross-section ×, kg/s
m_{ref}	reference mass of drive mechanism moving parts, kg
N_B	Beale number $= \zeta_{B,\max} = P_{B,\max}/\left(p_m V_{sw} n^*_{s,\max}\right)$
N_{MA}	characteristic Mach number $= n_s V_{sw}^{1/3}/\sqrt{RT_{wC}}$
$N^*_{MA,\max}$	characteristic Mach number under maximum brake power conditions $= n^*_{s,\max} V_{sw}^{1/3}/\sqrt{RT_{wC}}$
$N_{MA,\max}$	characteristic Mach number under maximum indicated power conditions $= n_{s,\max} V_{sw}^{1/3}/\sqrt{RT_{wC}}$
N_m	characteristic drive mechanism number $= m_{ref} RT_{wC}/(p_m V_{sw})$
N_p	characteristic pressure number $= p_m V_{sw}^{1/3}/(\mu\sqrt{RT_{wC}})$
N_{SG}	characteristic Stirling number $= p_m/(\mu n_s)$
N_{ST}	Stanton number
N_{TCR}	characteristic regenerator thermal capacity number
N_{α_R}	characteristic regenerator thermal diffusivity number
n_s	engine speed, rev/s
$n_{s,\max}$	engine speed at maximum indicated power, rev/s
$n^*_{s,\max}$	engine speed at maximum brake power, rev/s
P_B	brake power, W
P_{ind}	indicated power, W
p	pressure, Pa
p_{me}	mean effective pressure, Pa
p_m	mean pressure, Pa
$\dot{Q}_C$	thermal power in the cooler, W
$\dot{Q}_E$	thermal power in the heater, W
R	specific gas constant, J/(kg·K)
r_{hx}	hydraulic radius of space ×, m
T_{wC}	cooler wall temperature, K
T_{wE}	heater wall temperature, K
V_{dx}	dead volume of space ×, m^3
V_{MO}	volume of maximum overlapping, m^3
V_{sw}	swept volume, m^3
v	instantaneous volume, m^3
$\alpha, \beta, \chi, \delta$	parameters of mechanical power losses
α	phase angle, rad
α_{wx}	dimensionless wetted area of space × $= A_{wx}/V_{sw}^{2/3}$
Φ	coefficient of lineal indicated power losses
γ	adiabatic coefficient of working fluid
κ	swept volume ratio $= V_C/V_E$
$\lambda_1, \cdots, \lambda_k$	dimensionless geometric parameters of the gas circuit, including those characteristic of the drive mechanism
λ_{hx}	dimensionless hydraulic radius of space × $= r_{hx}/V_{sw}^{1/3}$
μ	working fluid viscosity at reference temperature, Pa·s
μ_L	lubricating viscosity at reference temperature, Pa·s
μ_{dx}	dimensionless dead volume of space × $= V_{dx}/V_{sw}$
Ψ	coefficient of quadratic indicated power losses
θ	crank angle, rad
τ	temperature ratio $= T_{wC}/T_{wE}$
ζ_B	dimensionless brake power $= P_B/(p_m V_{sw} n_s)$
ζ_{ind}	dimensionless indicated power $= P_{ind}/(p_m V_{sw} n_s)$
ζ_{mec}	dimensionless mechanical power losses $= \zeta_{ind} - \zeta_B$
ζ_0	quasi-static dimensionless work per cycle $= W_0/(p_m V_{sw})$

Subscripts

C, c	compression or cold space
cor	correlation prediction
E, e	expansion or hot space
exp	experimental value
max	under maximum power conditions
R	regenerator
xc	cooler
xe	heater

this allows its adaptation to various applications with highly competitive levels of chemical and noise pollution. This may explain why, apart from cryogenics [1], the most successful applications of Stirling cycle machines have so far been in AIP submarines, where Stirling engines are perhaps the most mature technology [2], solar energy conversion [3], waste heat recovering [4,5], co-generation [6–8] and tri-generation [9,10], mainly at low power scale.

During recent decades, research on Stirling engines has been progressing and computer advances have allowed models with simplifying hypotheses more applicable to the reality of physical phenomena. New prototypes have also been developed, comparing their operation with simulations using particular thermodynamic models, but the published reports do not always contain sufficient information to facilitate their analysis using independent author models. A priori, it cannot be guaranteed that a model suitable for one engine will provide good results for others. Conventional thermodynamic models have recently been compared with experimental results from the GPU-3 engine [11]. Power prediction errors were less than 5% in 2 cases, but wide differences ranging from 20% to 180% were observed in the remaining 10 cases. The best results were obtained with a polytropic model [12], but other models may be acceptable for other prototypes.

The use of dimensionless variables is interesting in all application areas of the technique, both for the simulation and optimization of designs and for the analysis of experimental results. In the area of Stirling engines, Finkelstein's pioneering work on the thermodynamic cycle merits highlighting [13]. Organ produced an exhaustive description of the physical phenomena involved in the gas circuit of a Stirling machine and identified a complete set of dimensionless variables influencing the indicated power and efficiency, thereby justifying dynamic

similarity criteria [14,15]. Other authors have corroborated this approach for kinematic engines [16] and thermoacoustic machines [17]. Prieto and co-workers made explicit the influence of engine speed on the indicated power model [18–20] and extended the description to the set of variables that influence brake power [21]. Recent works have analysed particular characteristics of free-piston engines [22] and the ranges in which real gas effects can be expected [23].

Procedures based on dimensionless variables can be used as generalised analysis tools or as a basis for preliminary design, using scaling techniques applied to operating data of reference engines [24–26]. Some researchers have considered that scaling-based design has limited possibilities, owing to the restrictions derived from geometric similarity [27]. Occasionally these limitations are mitigated by applying criteria of relaxed similarity to a prototype [28], but design options certainly increase if generalised correlations based on experimental data of prototypes are available. Such correlations can provide at the preliminary design stage a useful starting point for further optimisation tasks, in which advanced models and numerical methods may be needed to estimate variables whose measurement is practically unworkable [29]. In addition, generalised correlations could be used to validate simulation codes if they fit a wide variety of benchmark engines with acceptable accuracy.

The first correlation obtained from Stirling engines of various characteristics has given rise to the so-called 'Beale number'. This concept has played a vital role in the advancement of Stirling engine technologies and is frequently cited as a useful criterion for the preliminary design, even in works that demonstrate the complexity of the thermodynamic analysis of the gas circuit [30,31], but many engines deviate from the typical value ($N_B \approx 0.15$). Predictions as far from said value as $N_B \approx 0.35$ have also been obtained at high temperature level from parametric simulations carried out with commonly accepted programs [32], but experimental corroborations have not been published yet. West's number attributes variations in Beale's number to the temperature ratio, but there are many other influential variables. On the other hand, both Beale and West numbers need to be complemented with a correlation of engine speed. A variant of West's number, complemented by a dimensionless speed equation as a function of 5 influential variables, was the first attempt to solve this problem [33]. The correlations were constructed from 6 operating points of 5 engines. Information on correlation errors has not been published by the authors, except graphs for high temperature level engines, with logarithmic scales that could distort their values. The small number of influential variables considered may explain the fact that other authors have observed notable deviations for different operating points [21,23].

This article introduces a method for constructing the equivalent thermodynamic cycle for each operating velocity and calculating the indicated power and mechanical efficiency, through generalised correlations of power and engine speed. The correlations previously introduced [23] are improved by the influential variables selected, the amount and variety of experimental data available, and the use of non-lineal regression based on least squares of the relative errors. The validity of correlations is discussed by comparing their predictions with operating data of prototypes with kinematic drive mechanism.

2. Influential variables and basic equations

2.1. Gas circuit description

The indicated efficiency and dimensionless power of a Stirling engine with a kinematic drive mechanism depend on the set of dimensionless variables listed in the argument of the following functional relationship [15,16,19]:

$$\eta_{ind}, \zeta_{ind} \approx \mathrm{f}(\tau, \kappa, \lambda_1, \cdots, \lambda_k, \mu_{dx}, \cdots, \alpha_{wx}, \cdots, \lambda_{hx}, \cdots, \gamma, N_p, N_{MA}, N_{\alpha_R}, N_{TCR}) \quad (1)$$

To explicitly describe the influence of the engine speed on the indicated power, the following semi-empirical equation has been proposed [20]:

$$\zeta_{ind} = \zeta_0 - \Phi N_{MA} - \Psi N_{MA}^2 \quad (2)$$

In this equation, ζ_0 is the dimensionless quasi-static work per cycle, i.e. a thermodynamic concept that represents the theoretical limit of the gas circuit performance, whereas N_{MA} is an operating characteristic variable that can be interpreted as a non-dimensional engine speed, and the coefficients Φ and Ψ are macroscopic representations of the indicated power losses associated with irreversibilities inherent to working gas friction and heat transfer. Variants of this equation could be applicable to other thermodynamic cycles.

In a Stirling cycle, ζ_0 depends on the temperature ratio τ, geometric parameters of the drive mechanism, and dead volumes, but not on the working fluid, mean pressure, or engine speed. The quasi-static work per cycle can be deduced by numerical calculation from the following definition:

$$W_0 = \oint p_0(\theta) \mathrm{d}V \quad (3)$$

where p_0 is the instantaneous pressure of the quasi-static cycle without leakage, which can be calculated by an appropriate equation of state (EOS). If real gas effects are possible, the reduced cooler temperature and mean pressure must be added as influential variables in equation (1). Some models use the Van der Waals EOS to consider possible real gas effects, but friction and heat transfer correlations consistent with such ranges of operation are not always available [23]. However, the ideal gas model is acceptable in most applications, which leads to the following expression:

$$p_0(\theta) = M\ R\ T_{wC} / [v_R(\theta)\ V_{sw}] \quad (4)$$

where the dimensionless reduced volume is defined as follows:

$$v_R(\theta) = \tau \frac{v_E(\theta)}{V_{sw}} + S + \frac{v_C(\theta)}{V_{sw}} \quad (5)$$

Several hypotheses can be established for the dimensionless reduced dead volume S [34]. A frequently used option is to assume that the dead volume is divided into three spaces: two isothermal regions at the respective hot source and cold sink temperatures, and the regenerator dead volume, with linear temperature variation, which is equivalent to assuming that all the regenerator dead volume is at the logarithmic mean temperature T_R. In this case, the dimensionless reduced dead volume satisfies the following expression:

$$S = \tau \frac{V_{dE}}{V_{sw}} - \frac{\tau \ln \tau}{1 - \tau} \frac{V_{dR}}{V_{sw}} + \frac{V_{dC}}{V_{sw}} \quad (6)$$

For harmonic drive mechanisms, W_0 can be obtained from the classical Schmidt model, variations on whose formulation have been proposed by Rinia and Du Pré, Creswick, Finkelstein, Martini, Walker, etc. Depending on the configuration type, different expressions can be obtained for the analytical solutions of this model, but it should be noted that equivalent equations may appear different if the same variables are not used. Solutions obtained through a particular formulation [18,34], for the three basic configurations, can be seen in Appendix A, which allows comparisons to be made with Walker's formulation [35] for the alpha-type configuration.

After calculating ζ_0, the characteristic curves of indicated power can be obtained if the maximum power and its corresponding velocity are known, because equation (2) allows the coefficients Φ and Ψ to be calculated for each level of temperature and mean pressure using the following equations:

$$\Phi = \frac{2\zeta_0 - 3\zeta_{ind,\max}}{N_{MA,\max}} \tag{7}$$

$$\Psi = \frac{2\zeta_{ind,\max} - \zeta_0}{N^2_{MA,\max}} \tag{8}$$

These equations show the advantages that the availability of experimental correlations of $\zeta_{ind,\max}$ and $N_{MA,\max}$ can provide. It should be noted that negative values of Φ and have no physical meaning, because equation (2) implies that the ratio $\zeta_{ind,\max}/\zeta_0$ must be within the following range of variation:

$$\frac{1}{2} \le \frac{\zeta_{ind,\max}}{\zeta_0} \le \frac{2}{3} \tag{9}$$

On the other hand, the dimensionless indicated power can also be interpreted as the ratio between the effective mean pressure of the thermodynamic cycle and the mean pressure, as it can be written:

$$\zeta_{ind} = \frac{P_{ind}/(V_{sw}n_s)}{p_m} = \frac{p_{em}}{p_m} \tag{10}$$

The following equation allows the estimation, for each operating speed, of the 'effective' attenuation that the irreversibilities exert on the quasi-static pressure:

$$p_e(\theta) = p_m + \frac{\zeta_{ind}}{\zeta_0}(p_0(\theta) - p_m) \tag{11}$$

Then, the correlations of $\zeta_{ind,\max}$ and $N_{MA,\max}$ provide a method for constructing the equivalent thermodynamic cycle and calculating the indicated work for each engine speed by integrating the effective pressure. As shown in Fig. 1, the iterative procedure starts with a specified engine configuration, working gas, mean pressure, and operating temperatures, and continues with the assumption of geometrical parameters of the gas circuit and the drive mechanism. For each selected geometry, the dimensionless quasi-static power and other input variables of the correlations can be calculated, leading to corresponding values of maximum indicated power and engine speed. Once acceptable values are achieved, equations (2), (7), (8) and (11) allow to estimate the instantaneous mass flow rates, build a map of particle paths, and, with the help of heat transfer correlations, perform calculations of heat powers in the heat exchangers.

The procedure may be acceptable at the preliminary design stage, although the irreversibilities cause not only pressure attenuation but also phase shift, so that the actual pressure is between the quasi-static and effective pressure waves. For example, in Fig. 2, the quasi-static pressure, effective pressure, and actual pressure are compared for the SOLO V-160 engine operating with helium under the conditions of $T_{wE} \approx 625°C, T_{wC} \approx 63°C$, $p_m = 120$bar, and $n_s \approx 1517$rpm, for which it develops an indicated power of approximately 9065 W [36].

The correlations can be tools for analysis of simulation results or for preliminary design. In this case, the correlations can be used to guide the start of the project, generally reducing the computing time and limiting the specifications based on known experimental data. This scheme is in principle compatible with any existing simulation model, at least as a complementary tool.

2.2. Mechanical power losses

At each sliding or rolling element of an engine, forces influencing mechanical power losses depend on instantaneous pressure and inertia effects. In its turn, instantaneous pressure depends on all the parameters influencing the thermodynamic cycle, while the instantaneous velocity is determined by the mean engine speed n_s and the geometrical parameters of the drive mechanism. Moreover, variations of local velocities and forces may cause different lubrication regimes to occur during a stroke, even if the rotational speed of the crankshaft is constant. Consequently, friction coefficients at mid-stroke and near the dead centres, for example, can be very different. The dimensionless local mechanical power losses can therefore be expected to have a dependence on velocity analogous to Stribeck's curve [21], in which the coefficient of friction depends on the Hersey number. In fact, it is easy to deduce that the dimensionless power caused by tangential friction in a cylindrical bearing is proportional to the coefficient of friction. The consistency of this approach with measurements in piston rings of internal combustion reciprocating engines [37], the analogy between the Hersey number and the inverse Stirling number, and the analysis of available experimental data from a variety of prototypes, justified that the following empirical equation has been proposed to express the mechanical power losses of Stirling engines, on a global scale [21]:

$$\zeta_{mec} = \alpha \exp\left(-\beta N_{SG}^{-1}\right) + \chi + \delta N_{SG}^{-1} \tag{12}$$

This equation can be used to identify the existence of leakage at low engine speeds, as the derived mechanical power losses would be proportional to the Stirling number. On the other hand, an additional term could be included in the equation to consider possible aerodynamic power losses such as those caused by a flywheel, which would be proportional to the square of the inverse Stirling number [21].

The inverse Stirling number is the natural dimensionless velocity from the viewpoint of analysing mechanical power losses, but it can be substituted in the equation by considering that $N_{MA} = N_p/N_{SG}$.

The coefficients of this equation can vary depending on the operating conditions, physical properties of the gas and regenerator material, geometric parameters related to the gas circuit and the drive mechanism, as well as the masses and moments of inertia of the moving elements. For a given engine operating with different gases, these can be written:

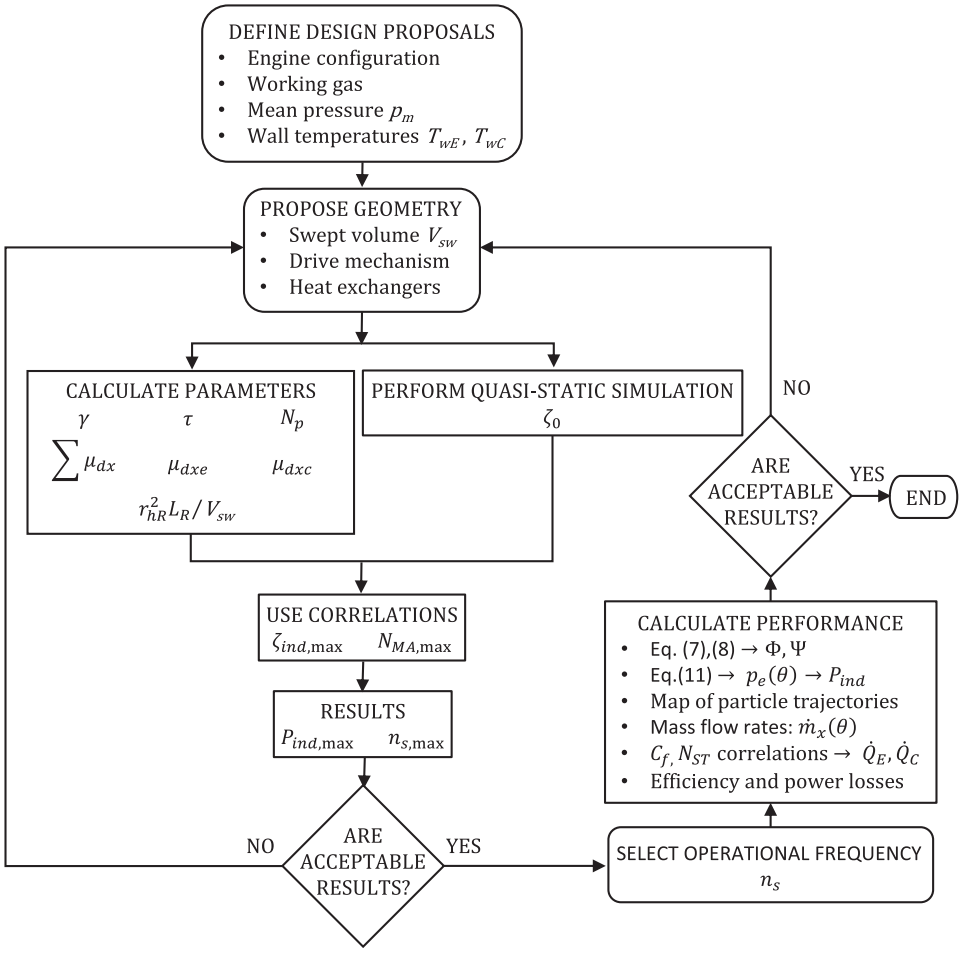

Fig. 1 Flow chart of preliminary gas circuit design.

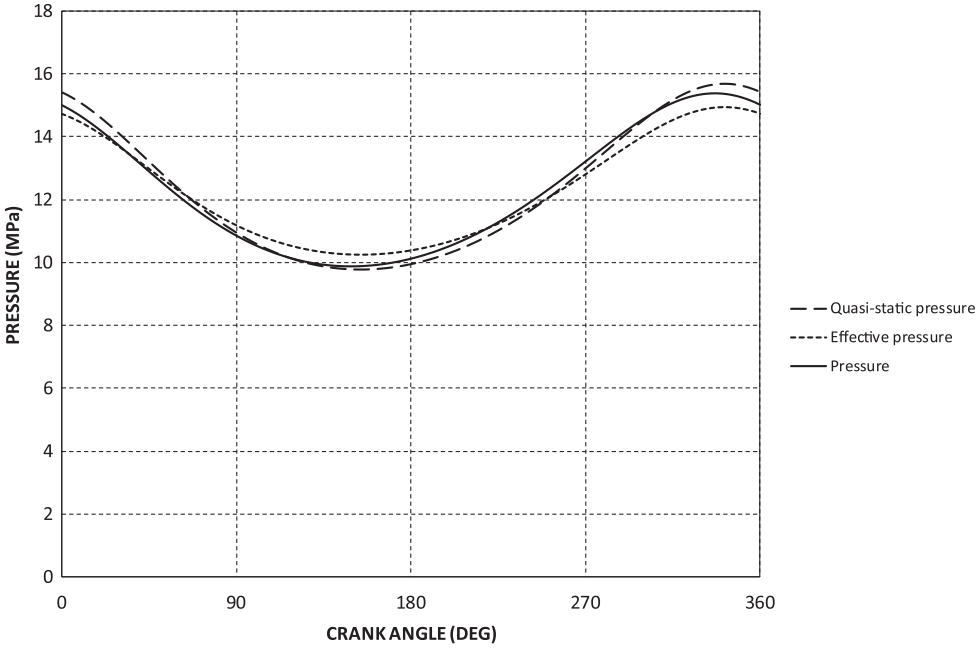

Fig. 2 Comparison of quasi-static, effective, and actual pressures for the SOLO V-160 engine.

$$\alpha,\ \beta, \chi,\ \delta \approx \mathrm{f}\left(\tau, \gamma, \frac{\mu_L}{\mu}, N_m, N_p\right) \tag{13}$$

In all the engines analysed so far, satisfactory results have been obtained by expressing these coefficients through potential functions of the following type:

$$\alpha, \chi, \delta \approx a_i \frac{N_m^{a_j}}{N_p^{a_k}}\ ;\ \beta \approx \frac{a_l}{(\mu_L/\mu)^{a_m}} \tag{14}$$

where the 11 numerical coefficients and exponents a_i can vary only with the type of gas and the temperature ratio.

3. Revision of correlations

The following 21 operating conditions corresponding to experimental data series of 8 Stirling engines of varying size and characteristics were previously analysed to obtain correlations for the dimensionless values of the maximum indicated and brake power and their corresponding velocities [23]:

- GPU-3 engine with hydrogen and helium both at $T_{wE} = 977$K and $p_m = 27.6$bar.
- M102C engine with air at $T_{wE} = 1073$K and seven p_m values: 12.41, 11.03, 9.66, 8.28, 6.90, 5.52, and 4.14 bar.
- P-40 engine with hydrogen, helium and nitrogen at $T_{wE} = 1023$K and $p_m = 150$bar.
- V-161 engine with hydrogen at $T_{wE} = 1005$K and $p_m = 112.2$bar.
- V-160 engine with helium at $T_{wE} = 898$K and five p_m values: 120, 100, 80, 60, and 40 bar
- Ecoboy engine with air at $T_{wE} = 703$K and $p_m = 8$bar.
- Yamanokami-1 engine with air at $T_{wE} = 403$K and $p_m = 1$bar.
- Yamanokami-2 engine with air at $T_{wE} = 368$K and $p_m = 7$bar.

To select the influential variables, two requirements were imposed, namely that the variables are not numerous, for reasons of simplicity, and that they are relevant parameters at the preliminary design stage. Because several dozen variables are implicit in equations (1) and (12), it is necessary to assess the degree to which these criteria compromise the accuracy of the correlations.

The correlations were based on the adjustment criterion of minimising the root mean square errors according to the following definition:

$$\mathrm{RMSE} = \sqrt{\frac{1}{n}\sum \left(X_{cor} - X_{exp}\right)^2} \tag{15}$$

where X represents the analysed variable and n is the number of data.

A subsequent analysis of the results suggested considering the variability of experimental data, as, for example, an absolute error equal to $X_{cor} - X_{exp} = 0.005$ would mean a relative error of 2% for $X_{exp} = 0.25$, whereas the relative error would be 20% for $X_{exp} = 0.025$. Therefore, the correlations have been revised not only by considering other possible influential variables and adding new experimental data, but also by using the criterion of minimising the relative root mean square errors, with the complementary information of the relative mean bias error, according to the following definitions:

$$\mathrm{RRMSE} = \sqrt{\frac{1}{n}\sum \left(\frac{X_{cor} - X_{exp}}{X_{exp}}\right)^2} \tag{16}$$

$$\mathrm{RMBE} = \frac{1}{n}\sum \left(\frac{X_{cor} - X_{exp}}{X_{exp}}\right) \tag{17}$$

3.1. Maximum indicated power

The criterion of minimising the RMSE value led to the following correlation for $\zeta_{ind,\max}$ [23]:

$$\zeta_{ind,\max} \approx 2.249\, \zeta_0^{1.054} \left(\frac{r_{hR}}{L_R}\right)^{0.190} \tag{18}$$

For this equation, RRMSE = 9.14% and RMBE = 1.13% are obtained, with the maximum relative error (MRE) equal to 19.53% for the GPU-3 engine operating with helium. Keeping the same influential variables, the criterion of achieving the minimum value of RRMSE leads to the results shown for the first case study in Table 1.

The addition of influential variables leads to significantly improved correlation, as can be seen in Case 2 of Table 1. The inclusion of ζ_0 as a variable that influences $\zeta_{ind,\max}$ is justified by the variation interval established by equation (9) for the ratio $\zeta_{ind,\max}/\zeta_0$. Other variables included involve variables that do not influence ζ_0, such as γ and N_p, which represent physical properties of the working gas, as well as r_{hR}/L_R and α_{wxe}, which are geometric parameters related to mechanical and thermal irreversibilities in the regenerator and the heater. With respect to the variable $\sum \mu_{dx}$, it was included in the analysis after noting that it can improve the adjustments, although its influence is already somehow included in ζ_0.

3.2. Engine speed corresponding to the maximum indicated power

The criterion of minimising the RSME value led to the following correlation of $N_{MA,max}$ [23]:

$$N_{MA,\max} \approx 0.001913 (1-\tau)^{0.355} \left(\frac{r_{hR}}{L_R}\right)^{0.223} \gamma^{-0.220} \left(\sum \mu_{dx}\right)^{0.217} N_p^{0.146} \tag{19}$$

For this equation, RRMSE = 11.75% and RMBE = 1.58% are obtained, with MRE = 27.99% for the GPU-3 engine operating with hydrogen. Keeping the same influential variables, if the adjustment is made with the criterion of achieving the minimum RRMSE value, better values of RRMSE, RMBE, and MRE are obtained, as can be seen in Case 1 of Table 2.

In Case 2, ζ_0 has been included as a variable instead of $(1-\tau)$, given the proportionality between both variables as deduced from equation (A6). From a practical point of view, both correlations show similar accuracy.

3.3. Maximum brake power

The criterion of minimizing the RMSE value led to the following correlation of $\zeta_{B,\max}$ [23]:

Table 1 Comparison of correlations of dimensionless maximum indicated power.

Case No.	Tested equation	RRMSE (%)	RMBE (%)	MRE (%)	Engine
1	$\zeta_{ind,\max} \approx 1.3681\zeta_0^{1.118}\left(\frac{r_{hR}}{L_R}\right)^{0.099}$	7.18	–0.52	18.67	GPU-3/He
2	$\zeta_{ind,max} \approx 0.4920\zeta_0^{0.900}\left(\frac{r_{hR}}{L_R}\right)^{-0.009}\gamma^{-0.311}(\sum\mu_{dx})^{-0.331}N_P^{0.011}$	3.50	–0.12	8.70	Ecoboy

Table 2 Comparison of correlations of dimensionless engine speed corresponding to the maximum indicated power.

Case No.	Tested equation	RRMSE (%)	RMBE (%)	MRE (%)	Engine
1	$N_{MA,\max} \approx 0.001050(1-\tau)^{0.218}\left(\frac{r_{hR}}{L_R}\right)^{0.057}\gamma^{-0.472}(\sum\mu_{dx})^{0.109}N_p^{0.117}$	10.98	–1.21	20.67	GPU-3/H2
2	$N_{MA,\max} \approx 0.000541\zeta_0^{0.026}\left(\frac{r_{hR}}{L_R}\right)^{-0.071}\gamma^{-0.565}(\sum\mu_{dx})^{-0.003}N_p^{0.105}$	11.62	–1.35	22.51	V-161

$$\zeta_{B,\max} \approx 2.301\,\zeta_0^{1.087}\left(\frac{r_{hR}}{L_R}\right)^{0.119}N_p^{-0.039} \tag{20}$$

For this equation, RRMSE = 10.77% and RMBE = 0.69% are obtained, with MRE = 25.88% for the GPU-3 engine operating with hydrogen. Maintaining the same influential variables, if the adjustment is made with the criterion of achieving the minimum RRMSE value, somewhat better values of RRMSE and RMBE are obtained, with MRE = 22.74% for the GPU-3 engine operating with helium, as can be seen in Case 1 of Table 3. The results are improved in Case 2 of the table, as five influential variables are added.

3.4. Engine speed corresponding to the maximum brake power

The criterion of minimising the RMSE value led to the following correlation of $N^*_{MA,\max}$ [23]:

$$N^*_{MA,\max} \approx 0{,}00202(1-\tau)^{0.485}\left(\frac{r_{hR}}{L_R}\right)^{0.414}\gamma^{-0.493}\left(\sum\mu_{dx}\right)^{0.029}N_p^{0.220} \tag{21}$$

For this equation, RRMSE = 10.24% and RMBE = 0.54% are obtained, with MRE = 23.21% for the GPU-3 engine operating with hydrogen. If the adjustment is made with the criterion of achieving the minimum RRMSE value, maintaining the same influential variables, RRMSE = 8.99% and RMBE = − 0.81% are obtained, with MRE = 20.09% for the V-161 engine operating with hydrogen, as shown in Case 1 of Table 4. As in the cases in Table 2, a correlation with similar accuracy is obtained in Case 2, where ζ_0 is included as a variable instead of $(1-\tau)$.

4. Additional experimental data

Experimental data that were not used to obtain the correlations in the preceding section can be used to assess the validity of the corresponding equations. The analyses performed for the engines described below are examples of indirect characterisation, similar to those previously applied for other prototypes [38]. The success of the employed methodology depends on the number and variety of operating conditions available, as well as the quality of the measurements.

4.1. Analysis of the Philips M102C engine tests

For the Philips M102C engine, a total of 112 brake power measurements are available for 4 different temperatures, 4 rotational frequencies, and 7 mean pressures, which were already used in previous analyses with various objectives [20,21]. The case corresponding to 800 °C was previously used to construct equations (18), (19), (20), and (21) [23]. Using the same procedure, all the series of available measurements were analysed. As ζ_0 can be calculated numerically, the unknowns to be determined for each series of temperatures and mean pressure are the coefficients Φ and Ψ of equation (2) and the 11 coefficients or exponents a_i of equation (14). That is, there are 13 unknowns for each of the 4 temperature series.

The numerical results of the regressions are shown in Table 5 and in equations (22) to (25). Graphical comparisons between the experimental values and the predictions from the equations can be seen in Appendix B for the four series of temperatures, which demonstrate that high-quality

Table 3 Comparison of correlations of dimensionless maximum brake power.

Case No.	Tested equation	RRMSE (%)	RMBE (%)	MRE (%)	Engine
1	$\zeta_{B,max} \approx 1.1845\zeta_0^{1.139}\left(\frac{r_{hR}}{L_R}\right)^{0.210}N_p^{0.042}$	9.30	–0.61	22.74	GPU-3/He
2	$\zeta_{B,max} \approx 0.6774\zeta_0^{0.972}\left(\frac{r_{hR}}{L_R}\right)^{0.102}\gamma^{-0.062}(\sum\mu_{dx})^{-0.250}N_p^{0.024}$	8.18	–0.67	15.74	V-160

Table 4 Comparison of correlations of dimensionless engine speed corresponding to the maximum brake power.

Case No.	Tested equation	RRMSE (%)	RMBE (%)	MRE (%)	Engine
1	$N^*_{MA,\max} \approx 0.001223(1-\tau)^{0.259}\left(\frac{r_{hR}}{L_R}\right)^{0.193}\gamma^{-1.204}(\sum \mu_{dx})^{-0.091}N_p^{0.172}$	8.99	–0.81	20.09	V-161
2	$N^*_{MA,\max} \approx 0.000699{\zeta_0}^{0.105}\left(\frac{r_{hR}}{L_R}\right)^{0.087}\gamma^{-1.348}(\sum \mu_{dx})^{-0.121}N_p^{0.168}$	9.66	–0.93	19.80	GPU-3/H2

measured data are needed to make comparisons that have scientifically definable uncertainties.

For the series corresponding to $T_{wE} = 900°C$, good adjustments are obtained, with an average RRMSE of 3.04%, and the mechanical power losses can be expressed by the following equation:

$$\zeta_{mec} \approx 34.500\frac{N_m^{0.500}}{N_p^{0.512}}\exp\left(-\frac{7.466\cdot 10^9}{(\mu_L/\mu)^{0.020}N_{SG}}\right)+\frac{120.000}{N_m^{0.384}N_p^{0.332}} \quad (22)$$

The obtained adjustments are also good for the series at $T_{wE} = 800°C$, with an average RRMSE of 2.48%, and the mechanical power losses can be expressed by the following equation:

$$\zeta_{mec} \approx 30.000\frac{N_m^{0.500}}{N_p^{0.507}}\exp\left(-\frac{7.755\cdot 10^9}{(\mu_L/\mu)^{0.020}N_{SG}}\right)+\frac{137.000}{N_m^{0.389}N_p^{0.316}} \quad (23)$$

For the series at $T_{wE} = 700°C$, the mechanical power losses can be expressed by equation (24), with an average RRMSE of 5.15%. If series corresponding to 6.90 bar is excluded, which shows some measurement error, the average RRMSE is reduced to 3.30%.

$$\zeta_{mec} \approx 25.200\frac{N_m^{0.500}}{N_p^{0.507}}\exp\left(-\frac{7.755\cdot 10^9}{(\mu_L/\mu)^{0.020}N_{SG}}\right)+\frac{136.000}{N_m^{0.389}N_p^{0.315}} \quad (24)$$

In the case of the series at $T_{wE} = 600°C$, there is generally a greater dispersion of data, with values of Φ clearly greater than zero. For the total of seven series, the mechanical power losses can be expressed by equation (25), with an average RRMSE of 9.23%.

$$\zeta_{mec} \approx 28.600\frac{N_m^{0.500}}{N_p^{0.492}}\exp\left(-\frac{6.518\cdot 10^9}{(\mu_L/\mu)^{0.020}N_{SG}}\right)+\frac{140.000}{N_m^{0.375}N_p^{0.317}} \quad (25)$$

Table 5 Experimental data of the Philips M102C engine.

T_{wE}	ζ_0	p_m	$P_{B,\max}$	$n^*_{s,\max}$	Φ	Ψ	RRMSE	$P_{ind,\max}$	$n_{s,\max}$	$\zeta_{ind,\max}$	$N_{MA,\max}$
(°C)	(–)	(bar)	(W)	(rpm)	(–)	(–)	(%)	(W)	(rpm)	(–)	(–)
900	0.4303	12.41	489	1513	0	12,860	2.23	587	1542	0.2869	0.0033
		11.03	461	1570	0	11,760	3.87	546	1613	0.2869	0.0035
		9.66	369	1459	5	12,550	4.33	437	1501	0.2814	0.0033
		8.28	391	1710	0	9635	0.84	453	1782	0.2869	0.0039
		6.90	340	1773	0	8885	3.83	393	1855	0.2869	0.0040
		5.52	269	1745	0	9165	2.22	309	1827	0.2869	0.0040
		4.14	184	1593	0	11,000	3.96	212	1667	0.2869	0.0036
800	0.4041	12.41	409	1435	0	12,775	2.02	536	1500	0.2694	0.0032
		11.03	390	1496	0	11,575	3.86	501	1575	0.2694	0.0034
		9.66	360	1545	0	10,715	1.66	456	1637	0.2694	0.0035
		8.28	332	1632	0	9450	2.21	416	1743	0.2694	0.0038
		6.90	281	1640	0	9300	2.82	350	1757	0.2694	0.0038
		5.52	222	1609	0	9625	3.09	275	1728	0.2694	0.0037
		4.14	152	1463	0	11,675	1.68	187	1569	0.2694	0.0034
700	0.3745	12.41	287	1324	32	6335	3.64	408	1415	0.2170	0.0031
		11.03	290	1393	23	7195	0.35	396	1493	0.2249	0.0032
		9.66	281	1368	4	11,740	3.08	369	1454	0.2455	0.0031
		8.28	257	1411	2	11,270	2.37	331	1510	0.2475	0.0033
		6.90	233	1966	37	90	16.23	319	2295	0.1884	0.0050
		5.52	171	1392	5	10,705	3.03	217	1507	0.2443	0.0033
		4.14	116	1288	32	6335	7.34	148	1401	0.2386	0.0030
600	0.3406	12.41	190	1178	17	12,250	7.19	341	1208	0.2123	0.0026
		11.03	202	1265	14	10,905	18.54	329	1305	0.2139	0.0028
		9.66	194	1299	14	10,005	13.88	299	1355	0.2134	0.0029
		8.28	168	1280	18	9135	1.58	251	1353	0.2095	0.0029
		6.90	148	1274	18	8825	4.30	212	1372	0.2093	0.0030
		5.52	118	1229	20	8755	7.59	165	1348	0.2076	0.0029
		4.14	82	1120	24	9655	11.51	113	1246	0.2055	0.0027

In equations (22) to (25), the variations of numerical parameters may be due to uncertainties of the experimental procedure and the influence of the temperature ratio, as provided in equation (13). However, the influence of the temperature ratio seems to be small, as can be seen in Appendix C.

4.2. Analysis of the ST05G engine

The ST05G engine has a gamma configuration with dual-crank drive mechanism and $V_{sw} = 425.59\text{cm}^3$, and is designed to operate with nitrogen. Two brake power curves have been published for this engine [39], operating at the respective temperatures of $T_{wE} = 650°\text{C}$ and $T_{wE} = 450°\text{C}$, both for $T_{wC} = 15°\text{C}$ and a mean pressure of 10 bar. Indicator diagrams corresponding to the rotational frequency of 500 rpm have also been published for the same temperature and pressure conditions.

The power curves for each series have been deduced from the brake power measurements by the same indirect characterisation procedure as used for the M102C engine. Assuming that the same values of the parameters a_i of equation (14) are applicable for both series, the mechanical power losses can be expressed by the following equation and the experimental values of the brake power can be adjusted to the model with RRMSE = 3.89%:

$$\zeta_{mec} \approx 1.155 \frac{N_m^{0.168}}{N_p^{0.200}} \exp\left(-\frac{2.220 \cdot 10^{10}}{(\mu_L/\mu)^{0.023} N_{SG}}\right) + \frac{0.180}{N_m^{0.186} N_p^{0.008}} + 1.958 \cdot 10^7 \frac{N_m^{0.079}}{N_p^{0.057} N_{SG}} \quad (26)$$

Table 6 shows the results of the calculations and Fig. 3 shows a comparison of the experimental values with the characteristic curves defined by equations (2) and (12). The figure also shows that the solid lines of the indicated power roughly pass through the red symbols that represent the indicated power values calculated by integrating the indicator diagrams obtained experimentally at 500 rpm.

The ST05G engine has been the subject of other recent investigations. Maximum brake power values of 362 W at 679 rpm, 471 W at 752 rpm and 514 W at 800 rpm have been measured, operating with air at $p_m = 7\text{bar}$ and $T_{wE} = 500$, 600 and 700 °C, respectively [40]. For these operating conditions, the respective values of $\zeta_0 = 0.2250$, 0.2491 and 0.2697 have been calculated.

Numerical simulations aimed at engine optimization are also available [41], which allow estimating values of $P_{B,\max} = 313\text{W}$ and 575 W, both at 633 rpm, $T_{wE} = 500°\text{C}$ and $T_{wC} = 15°\text{C}$, with air at $p_m = 5$ and 10 bar, respectively, as well as values of $P_{B,\max} = 198\text{W}$ at 455 rpm, 329 W at 538 rpm and 478 W at 633 rpm, operating with air at $p_m = 8\text{bar}$, for the respective temperatures of $T_{wE} = 300$, 400 and 500 °C. For these operating conditions, the respective values of $\zeta_0 = 0.1685$, 0.2034 and 0.2319 have been calculated.

Additional data can also be obtained from the ST05G unit that has been installed at the University of Oviedo in order to evaluate its operation with energy supply through a commercial biomass boiler (Fig. 4). The experimental results, operating with nitrogen at $p_m = 5.3\text{bar}$, $T_{wE} = 420°\text{C}$ and $T_{wC} = 23°\text{C}$, lead to $P_{B,\max} = 156\text{W}$ at 494 rpm [42]. For this operating condition, the value $\zeta_0 = 0.2038$ has been calculated.

5. Discussion

5.1. Correlations for maximum indicated power

For the 21 data used as a basis for the correlation in Case 2 of Table 1, the greatest deviations correspond to the Ecoboy engine (−8.70%) and the Yamanokami-1 engine (+7.80%). Most of the 21 values of the M102C engine that were not used in the correlations, that is, those corresponding to the operating conditions of 600, 700, and 900 °C, are included in the ± 10% deviation range. The value furthest from the correlation corresponds to 700 °C and 6.90 bar, with a deviation of + 32.25% that corroborates the already mentioned doubtfulness of the validity of this value. For the ST05G engine, the deviations are − 17.95% and − 14.69%, respectively, under the first two operating conditions mentioned in the previous section.

Based on these results, it was considered interesting to expand the dataset used to construct the correlation by including these two data from the ST05G engine. To balance the contributions of the various prototypes, only three V-160 engine data were added, at p_m values of 120, 80 and 40 bar, whereas only four M102C engine data were included, at T_{wE} values of 1073 K and 1173 K, and p_m values of 12.41 and 4.14 bar.

In the first instance, the same influential variables assumed in Case 2 were considered, however, better results were obtained after replacing the r_{hR}/L_R ratio by the following parameter, which implicitly includes more geometric properties related to the thermodynamic behaviour of the regenerator:

$$\frac{r_{hR}^2 L_R}{V_{sw}} = \left(\frac{r_{hR}}{L_R}\right)^2 \cdot \left(\frac{L_R}{V_{sw}^{1/3}}\right)^3 = \frac{\mu_{dR}^3}{\alpha_{wR}^2 \cdot \alpha_{xR}} = \left(\frac{\mu_{dR}}{\alpha_{wR}}\right)^2 \cdot \frac{\mu_{dR}}{\alpha_{xR}}$$

Deviations also decreased after the temperature and dead volume ratios of the heater and cooler were included as explicit influential variables, which does not mean using unknown parameters at the preliminary design stage. The following equation fits the 18 experimental data thus available with RRMSE = 3.20% and RMBE = –0.17%:

$$\zeta_{ind,\max} = 0.8280 \zeta_0^{1.0716} \left(\frac{r_{hR}^2 L_R}{V_{sw}}\right)^{0.0209} \gamma^{-0.1696} \left(\sum \mu_{dx}\right)^{-0.0527} N_p^{0.0184} \tau^{0.1932} \mu_{dxe}^{-0.1012} \mu_{dxc}^{0.0518} \quad (27)$$

As can be seen in Fig. 5(a), all the data used as a basis for the correlation are included among the dashed lines that delimit deviations of ± 10% from the correlation. The limits of the relative deviations now correspond to the P-40 engine operating with hydrogen (+6.60%) and the ST05G operating at 650 °C (−6.35%). With respect to values used for the validation, the deviations are acceptable for the V-160 engine data and most of the M102C engine data, as shown in Fig. 5(b), except the value corresponding to 700 °C and 6.90 bar, which shows an even greater deviation (+34.55%) than in previous correlations. The correlation also conforms acceptably to the beta type engine designed by Philips to produce 400 BHP using a single gas circuit, with rhombic drive mechanism and $V_{sw} = 15000\text{cm}^3$, operating with helium at $p_m = 110\text{bar}$ and $T_{wE} = 694°\text{C}$ [43]. Taking into account that $\zeta_0 = 0.4310$ can be calculated for these operating conditions, the values of

Table 6 Analysis of maximum brake power and velocity for the ST05G engine.

T_{wE}	T_{wC}	p_m	ζ_0	$\zeta_{ind,\max}$	$N_{MA,\max}$	Φ	Ψ	$P_{ind,\max}$	$n_{s,\max}$	$P_{B,\max}$	$n^*_{s,\max}$
(°C)	(°C)	(bar)	(–)	(–)	(–)	(–)	(–)	(W)	(rpm)	(W)	(rpm)
650	15	10.0	0.2662	0.1644	0.00295	13.3	7199	802	688	508	600
450	15	10.0	0.2183	0.1323	0.00242	16.4	7905	530	565	260	500

$P_{ind,\max} \approx 325$kW at 430 rpm and $P_{B,\max} \approx 266$ kW at 450 rpm have been estimated, which are in agreement with Philips' specifications and tests.

5.2. Correlations for engine speed corresponding to maximum indicated power

In this case, the dispersion is greater than in the correlations of dimensionless maximum indicated power. Among the 21 data used as a basis for the correlation in Case 1 of Table 2, the greatest deviations correspond to the GPU-3 engine operating with hydrogen (+20.67%) and the SOLO V-161 engine (−18.56%). The value of $N_{MA,\max} \approx 0.0059$ considered for this prototype is the highest observed in Stirling engines to date, but it should be noted that it results from an extrapolation from an analysis of data from the SOLO V-160 engine operating with helium at nearly constant rotation frequencies [31], and thus it might be increased by uncertainties inherent in the estimation. With respect to data used for the validation, the values furthest from the correlation correspond to the M102C engine, operating in the already mentioned condition of 6.90 bar and 700 °C (−24.63%), and operating at various pressures of the 600 °C series, with deviations that may be greater than 40%. The deviations corresponding to the ST05G engine are even greater, especially at 450 °C (+74.60%).

Using the same influential variables assumed in Case 2 of Table 2, another correlation was obtained including the ST05G engine operating point at 650 °C, whereas keeping the value at 450 °C for validation purposes only. The following equation fits the 22 experimental data thus available with RRMSE = 12.04% and RMBE = − 1.38%:

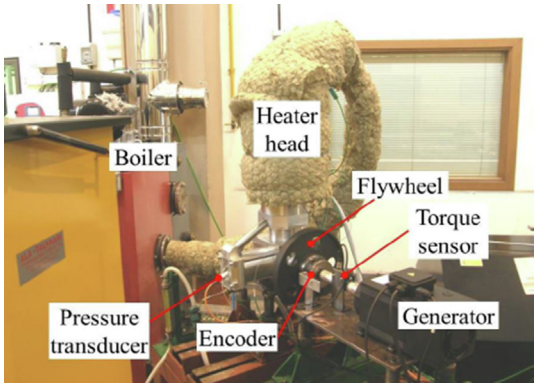

Fig. 4 Test rig with Stirling engine connected to the biomass boiler and the electrical generator.

$$N_{MA,\max} \approx 0.000479\zeta_0^{-0.061}\left(\frac{r_{hR}}{L_R}\right)^{-0.155}\gamma^{-0.579}\left(\sum \mu_{dx}\right)^{-0.123}N_p^{0.073} \tag{28}$$

For the data used as a basis of the correlation, the deviations are between those corresponding to the V-161 engine (−27.23%) and the Yamanokami-1 engine (+24.87%), and that of the ST05G engine at 650 °C improves markedly (+14.37%). With respect to values used for the validation, the M102C engine series have somewhat smaller deviations than in the previous cases, but that of the ST05G engine remains high at 450 °C (+40.83%).

Finally, an additional correlation was obtained for the same operating points and influential variables used in the construction of equation (27). The following equation fits the 18

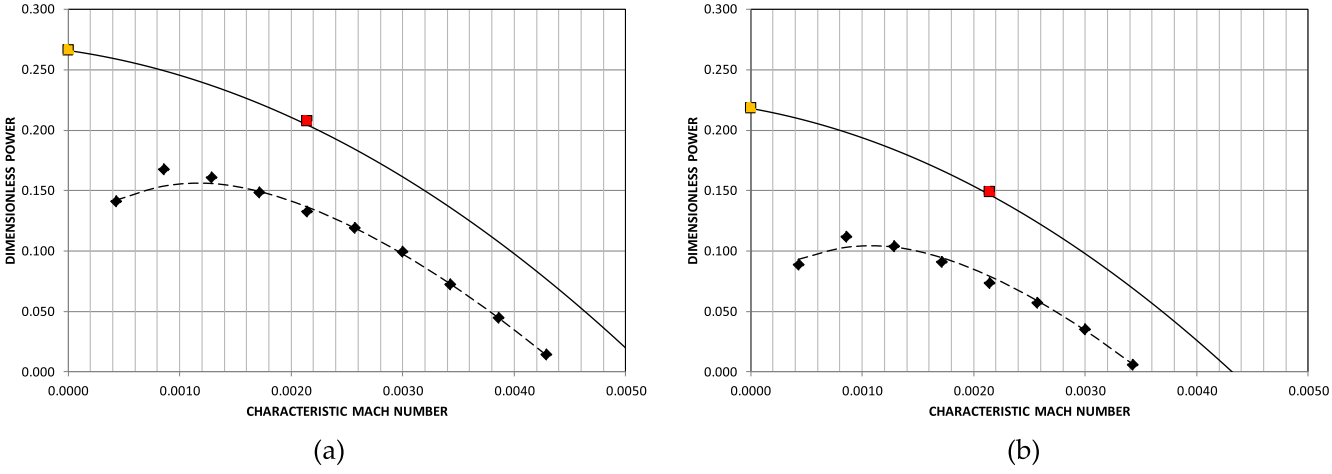

Fig. 3 Characteristic power curves of ST05G engine: (a)$T_{wE} = 650$°C; (b)$T_{wE} = 450$°C.

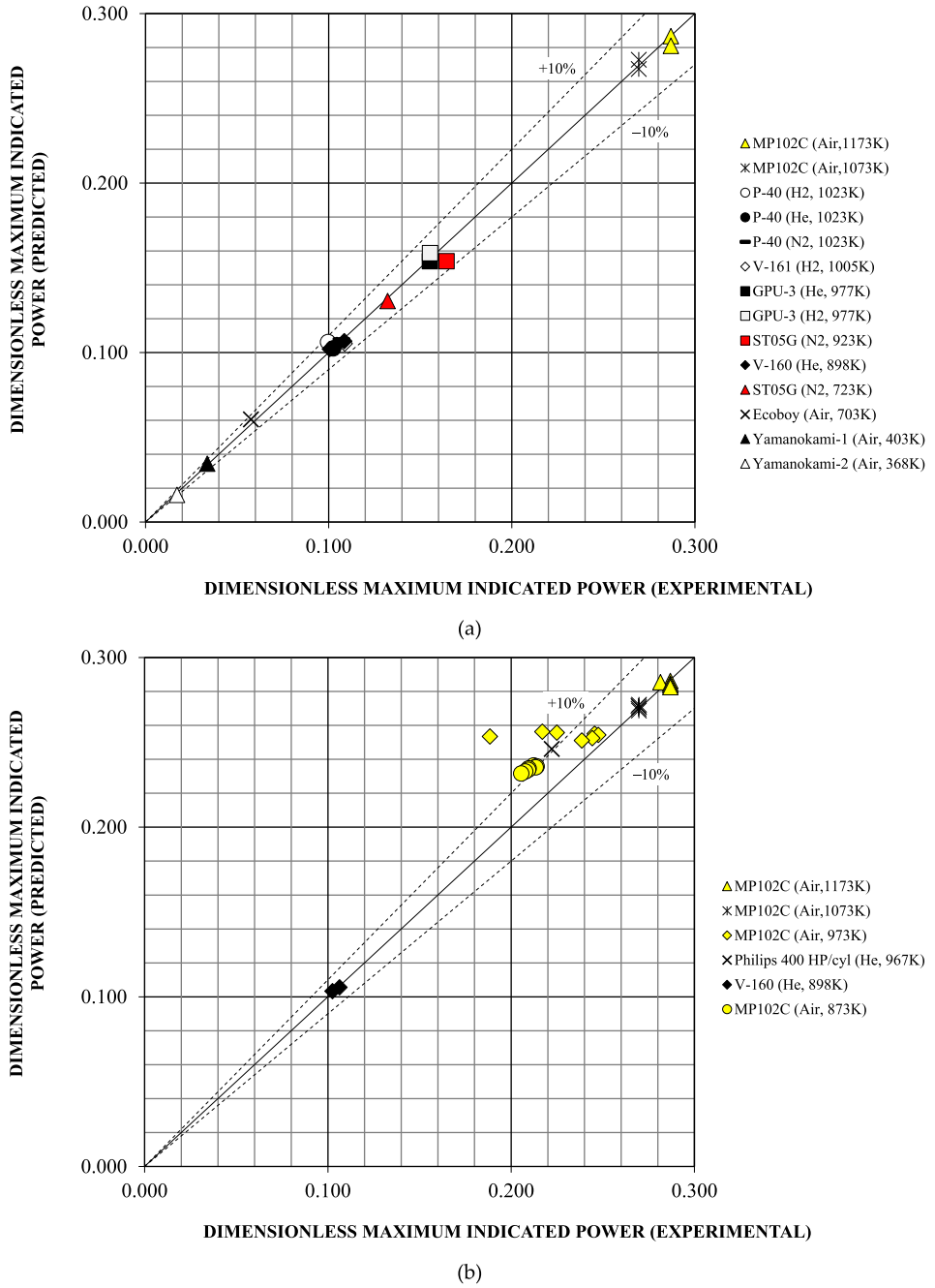

Fig. 5 Correlation for dimensionless maximum indicated power: (a) data used as a basis for the correlation; (b) data used for the validation.

experimental data with RRMSE = 6.35% and RMBE = 0.43%:

$$N_{MA,\max} = 0.000356\zeta_0^{-2.0664}\left(\frac{r_{hR}^2 L_R}{V_{sw}}\right)^{0.1131}\gamma^{-0.8828}\left(\sum\mu_{dx}\right)^{-1.8519}N_p^{-0.0106}\tau^{-2.7810}\mu_{dxe}^{0.5639}\mu_{dxc}^{0.0189} \quad (29)$$

As can be seen in Fig. 6(a), most of the data used as a basis for the correlation are included among the dashed lines that delimit deviations of ± 10% from the correlation. The limits of the relative deviations now correspond to the Yamanokami-2 engine (+11.00%) and the P-40 engine operating with nitrogen (−11.92%). With respect to values used for the validation, the deviations are acceptable for the V-160 engine data and most of the M102C engine data, as shown in Fig. 6(b). The deviation is almost negligible (−2.18%) for the P-400 HP/cyl project, whereas that of the M102C engine value corresponding to 700 °C and 6.90 bar (−42.64%) confirms the existence of measurement errors.

The analyses reflect the uncertainties inherent in any process of measurement and data processing. It seems easier to estimate the maximum power value than to accurately locate the corresponding speed, especially if the measurements are not numerous and are relatively dispersed, as occurs for exam-

ple in certain series of the M102C engine at 600 °C. This difficulty affects the deviations in both correlations of $\zeta_{ind,\max}$ and $N_{MA,\max}$.

The preliminary design criterion based on optimizing ζ_0 was recommended in previous publications [18,32], because it follows from equation (2) that $\zeta_{ind,\max}/\zeta_0 = 0.58 \pm 0.08$ whatever the parameters of a Stirling engine. This is in agreement with the low dispersion observed when comparing the variety of experimental data with the predictions of the $\zeta_{ind,\max}$ correlation.

Consequently, equation (27), and the complementary equation (29), can be useful for estimating with sufficient accuracy the indicated power expectations of an engine, by means of a not too high number of parameters available at the preliminary design stage.

5.3. Correlations for maximum brake power

For the 21 data used as a basis for the correlation in Case 2 of Table 3, it is observed that the majority are practically contained between the dashed lines that delimit deviations of ± 10%. The largest deviations correspond to the Ecoboy engine (−9.59%) and the V-160 engine (+15.74%). With respect to the operating points used for validation purposes,

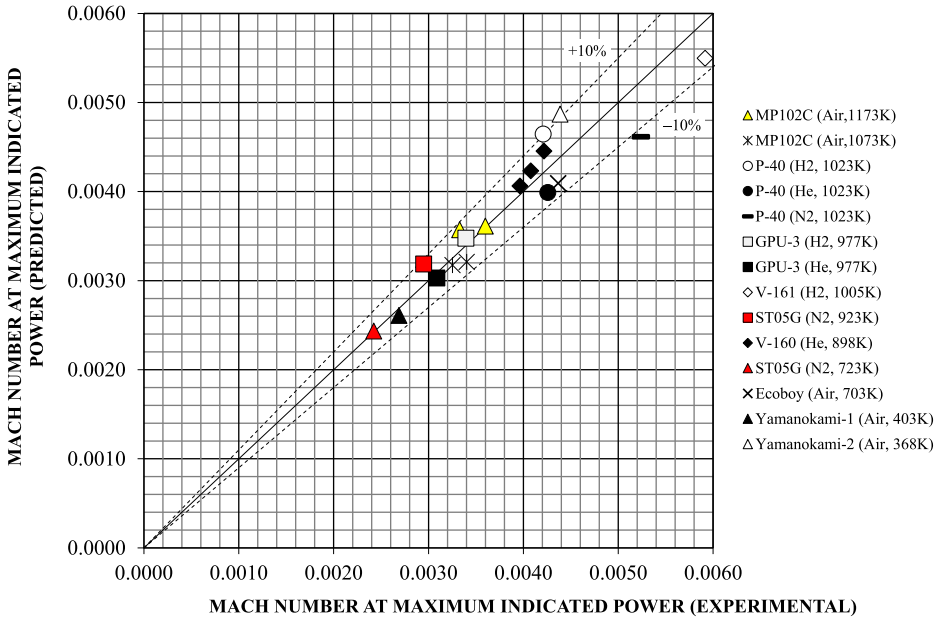

(a)

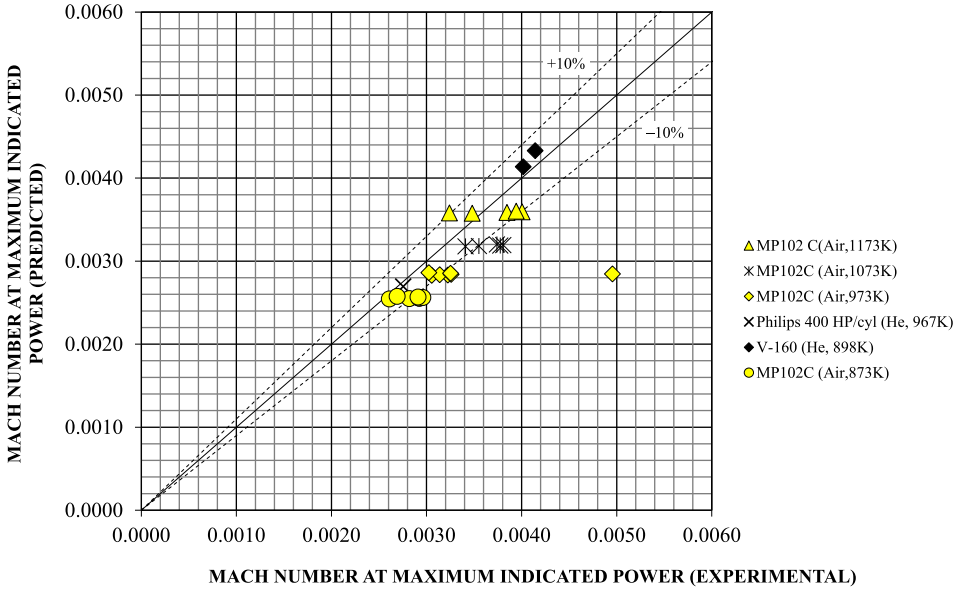

(b)

Fig. 6 Correlations for the characteristic Mach number at the maximum indicated power based on: (a) data used as a basis for the correlation; (b) data used for the validation.

it is observed that the data of the M102C engine at 900 °C and most values at 700 °C are consistent with the correlation. On the contrary, some values at 600 °C show deviations greater than 50%, which is consistent with the aforementioned dispersion presented by several measurements of these series. The value of the ST05G engine at 650 °C almost coincides with the prediction of the correlation, whereas the deviation is high at 450 °C (+37.25%).

Performing the analysis with the same operating points and influential variables used to construct the correlations of equations (27) and (29), an analogous correlation is obtained for all of the available engines. The following equation fits the 18 experimental data with RRMSE = 6.39% and RMBE = − 0.44%:

$$\zeta_{B,\max} = 0.8358\zeta_0^{-0.2918}\left(\frac{r_{hR}^2 L_R}{V_{sw}}\right)^{0.1123}\gamma^{-0.7655}\left(\sum\mu_{dx}\right)^{-1.6930}N_p^{-0.0406}\tau^{-1.2756}\mu_{dxe}^{0.4952}\mu_{dxc}^{-0.0429} \tag{30}$$

As can be seen in Fig. 7(a), most of the data used as a basis for the correlation are practically contained between the dashed lines that delimit deviations of ± 10%. The greatest deviations now correspond to the ST05G engine at 650 °C (−14.97%) and the P-40 engine operating with hydrogen (+14.81%), which is consistent with the observed divergences for the deviations of both engines in the $N_{MA,\max}$ correlation.

Fig. 7(b) shows a comparison of experimental data with the values predicted by this correlation for operating points used for validation purposes. Acceptable deviations are observed for the V-160 engine and for most M102C engine values at 700, 800 and 900 °C. The greatest deviation at 700 °C again corresponds to the mean pressure of 6.90 bar (+27.26%), but there are two values at 600 °C with greater deviations, which are assumed due to the already mentioned dispersion in these series. Regarding the ST05G engine, the data corresponding to 420 °C adjusts acceptably to the correlation (−10.24%), but the values corresponding to 500, 600 and 700 °C show deviations of the order of − 20%, which seem inconsistent with the rest of experimental measurements.

In the case of the Philips 400 HP/cyl project, the correlation predicts a value not too far from the specification (−16.74%). A similar deviation is obtained for the numerical simulation of the ST05G engine operating at 300 °C (−16.88%), but the remaining predictions are questionable, because they are greater than experimental values obtained at higher temperatures.

Equation (30) cannot achieve the accuracy of equation (27) because more variables influence on the brake power than on the indicated power, however it seems acceptable to explain the variability of $\zeta_{B,\max}$, that is, the Beale number, for the set of analysed engines. The remarkable difference (∼1700%) that exists between respective $\zeta_{B,\max}$ values of the M102C engine at 900 °C and the Yamanokami-2 engine at 95 °C evidences that the Beale number concept ($N_B \approx 0.15$) must be used with caution and that inter-engine comparisons based on relative errors are advisable.

5.4. Correlations for engine speed corresponding to maximum brake power

Even if the Beale number could be calculated as accurately as possible, such a concept becomes useless if the engine speed corresponding to the maximum brake power cannot be estimated. The comparison of the experimental results of the characteristic Mach number corresponding to the maximum brake power with the predictions from the equation of Case 2 of Table 4 shows that most of the data used as a basis for the correlation are between or very close to the ± 10% deviation limits, which correspond to the GPU-3 engine operating with hydrogen (+19.80%) and the P-40 engine operating with helium (−15.14%). The value of $N^*_{MA,\max}$ of the V-161 engine fits the correlation quite well, unlike the results of the analogous correlation for $N_{MA,\max}$. With respect to data used for the validation, the majority of M102C engine values show acceptable deviations, except for the value at the already mentioned conditions of 6.90 bar and 700 °C (−25.73%), and certain values of the 600 °C series. Much greater deviations are obtained for the ST05G engine data at 650 °C (+41.60%) and particularly at 450 °C (+64.12%).

As in the $N_{MA,\max}$ correlation case, an additional correlation was obtained including the ST05G engine operating point at 650 °C, whereas keeping the value at 450 °C for validation purposes only. The following equation fits the 22 experimental data with RRMSE = 10.26% and RMBE = − 1.00%:

$$N^*_{MA,\max} \approx 0.000588\zeta_0^{0.001}\left(\frac{r_{hR}}{L_R}\right)^{0.004}\gamma^{-1.390}\left(\sum\mu_{dx}\right)^{-0.259}N_p^{0.138} \tag{31}$$

For the data used as a basis for this correlation, most values have adjustments close to the previous cases, except for the V-161 engine, which marks one of the limits of the deviations (−17.38%), and the Ecoboy engine, with a similar deviation (−17.23%). The V-160 engine marks the other limit of the deviations operating at 40 bar (+14.89%), whereas the adjustment is good for other pressures. With respect to data used for the validation, the deviations of the M102C engine data operating at 600 °C are similar to those obtained in Case 2 of Table 4. As for the ST05G engine, the deviation at 650 °C is moderate (+14.85%) and that at 450 °C is markedly reduced compared to the previous correlation, although it is still high (+37.80%).

The analysis evidences the difficulty of obtaining a good correlation applicable to all the operating points, as in the $N_{MA,\max}$ correlation case. Thus, an additional correlation was obtained for the same operating conditions and influential variables used in the construction of equations (27), (29) and (30). The following equation fits the 18 experimental data available with RRMSE = 10.93% and RMBE = − 5.15%:

$$N^*_{MA,max} \approx 0.000220\zeta_0^{-1.0846}\left(\frac{r_{hR}^2 L_R}{V_{sw}}\right)^{0.0322}\gamma^{-1.5436}\left(\sum\mu_{dx}\right)^{-0.9204}N_p^{0.0500}\tau^{-1.6547}\mu_{dxe}^{0.1708}\mu_{dxc}^{-0.0178} \tag{32}$$

As can be seen in Fig. 8(a), most of the data used as a basis for the correlation are included among the dashed lines that delimit deviations of ± 10% from the correlation. The limits of the relative deviations now correspond to the V-160 engine at the mean pressure of 40 bar (+18.87%) and the V-161 engine (−17.21%). With respect to values used for the validation, the deviations seem acceptable for both V-160 and M102C engines, except again for the value of this engine corresponding to 700 °C and 6.90 bar (−36.04%), as shown in Fig. 8(b). The deviation of the ST05G engine data at 420 °C (−4.64%) is consistent with the values at 450 and 650 °C,

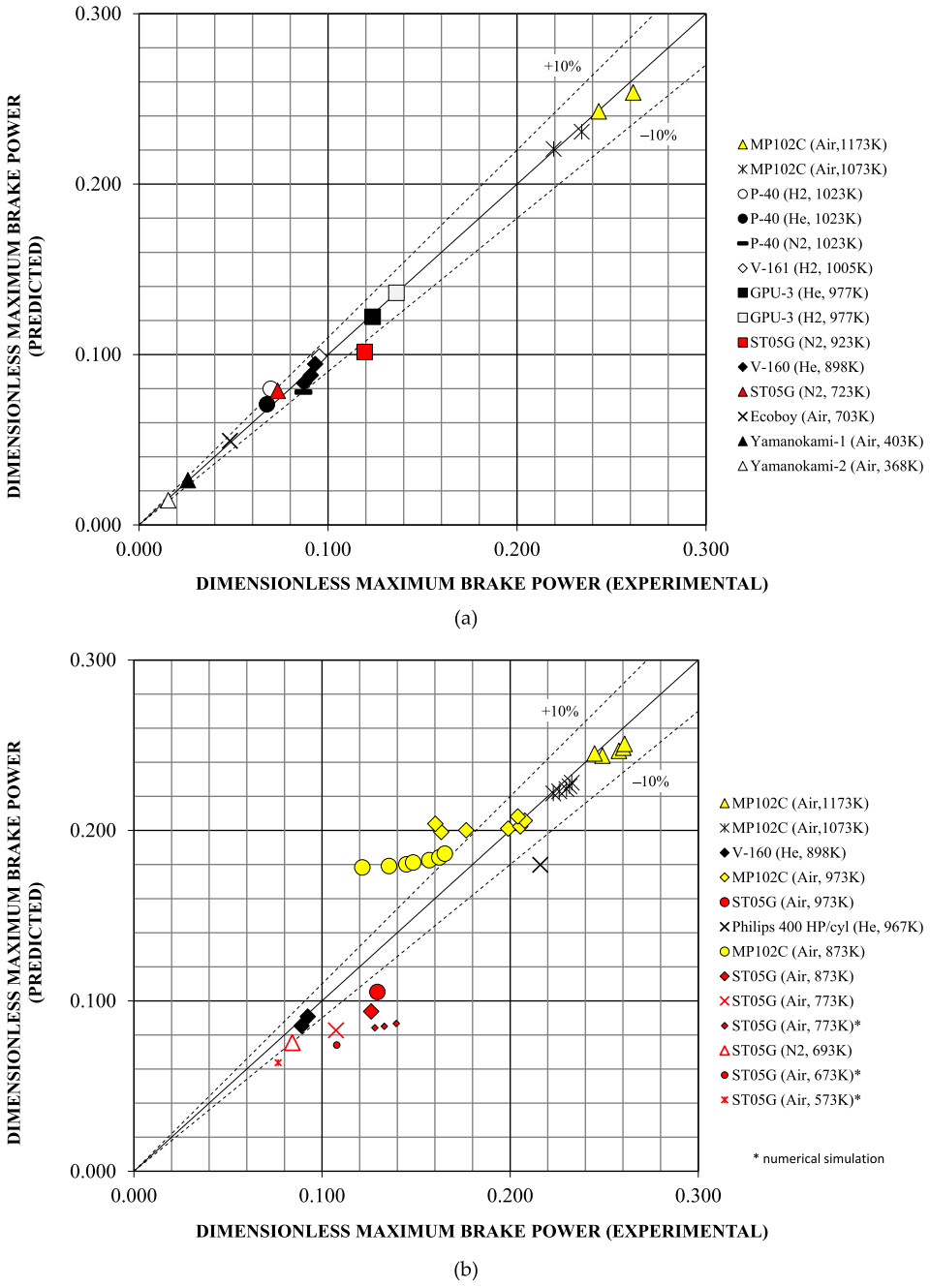

Fig. 7 Correlations for the dimensionless maximum brake power based on: (a) data used as a basis for the correlation; (b) data used for the validation.

but data at 500, 600 and 700 °C show deviations of the order of − 25%, which again seem inconsistent with the rest of independent experimental measurements and should be the subject of future research. Regarding the numerical simulations, the deviations are closer to the limits than in the correlation of equation (30), particularly at 300 °C (−3.66%). For the Philips 400 HP/cyl project, the correlation predicts a somewhat greater value than specified (+14.86%).

In summary, previous design criteria based on experimental averages of $N^{*}_{MA,\max}/N_{MA,\max}$ ratio and mechanical efficiency [21,34] can be improved by equations (30) and (32), but experimental performance data and characteristics of more prototypes are desirable to facilitate future updates of the proposed correlations or other variants aimed at generalised prototype analysis.

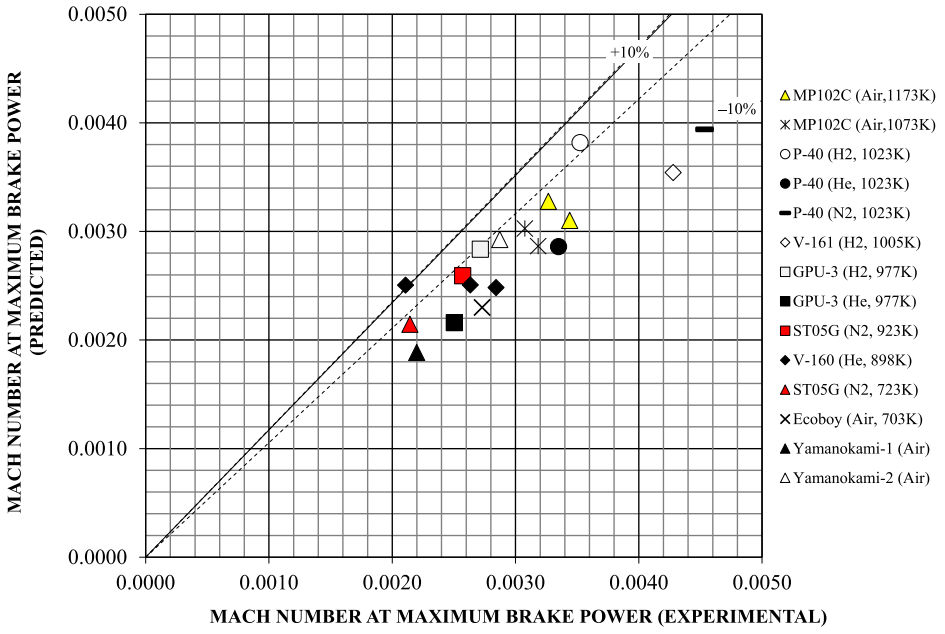

(a)

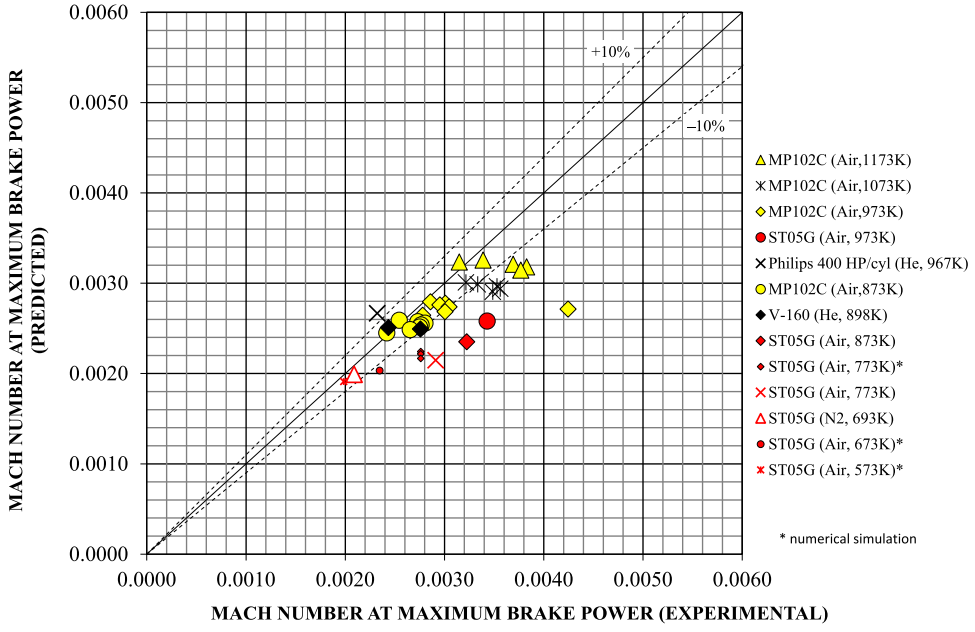

(b)

Fig. 8 Correlations for the characteristic Mach number at the maximum brake power based on: (a) data used as a basis for the correlation; (b) data used for the validation.

6. Conclusions

Experimental data of $\zeta_{B,\max}$, usually known as the Beale number, may differ by a factor proximate to 15, so it is recommended to use the classical correlation ($N_B \approx 0.15$) with caution. On the other hand, $\zeta_{B,\max}$ data from well-known engines are less than 0.27 so far, thus higher values predicted by numerical simulations are pending experimental confirmation.

Correlations for the engine speed corresponding to the maximum indicated and brake power are needed to complement $\zeta_{ind,\max}$ and $\zeta_{B,\max}$ correlations.

Correlations have been updated for a total of 10 engines of various size and characteristics, with the criterion of minimising relative errors in the regression analyses, using additional experimental data and selecting influential variables.

Correlations have acceptable accuracy in most cases using the following eight influential variables: the quasi-static dimensionless work per cycle ζ_0, ratio between the square of the hydraulic radius, multiplied by the length of the regenerator, and the engine swept volume $r_{hR}^2 L_R / V_{sw}$, adiabatic coefficient of the working gas γ, dimensionless dead volume of the total engine spaces $\sum \mu_{dx}$, characteristic pressure number N_p, and

temperature and dead volume ratios of the heater and cooler, i.e. τ, μ_{dxe} and μ_{dxc}.

The correlations of $\zeta_{ind,\max}$ and $N_{MA,\max}$ allow constructing the equivalent thermodynamic cycle and estimating the indicated power for any operating condition, while the mechanical efficiency can be calculated from the correlations of $\zeta_{ind,\max}$ and $\zeta_{B,\max}$.

Declaration of Competing Interest

The authors declare that they have no known competing financial interests or personal relationships that could have appeared to influence the work reported in this paper.

Acknowledgements

This research was co-financed by the European Union, through the ERDF Funds, and the Principality of Asturias, through the Science, Technology and Innovation Plan 2013-2017, grant number GRUPIN-095-2013.

Appendix A. Comparison between Schmidt's model formulations.

Table A1 shows the solutions obtained with a particular formulation [18,34] for the three basic configurations.

In these equations, the crank angle reference ($\theta = 0$) is the top dead centre of the compression piston stroke ($v_C = 0$ for an alpha-type engine). Moreover, p_{am} denotes the arithmetic mean of the cycle pressure, i.e. $p_{am} = (p_{\max} + p_{\min})/2$, and δ is half the cycle pressure amplitude normalized by p_{am}. Thus, it can be written:

$$\delta = \frac{p_{\max} - p_{\min}}{2p_{am}} = \frac{\Delta p}{2p_{am}} \tag{A1}$$

$$p_{\max} = p_{am}(1 + \delta) \tag{A2}$$

$$p_{\min} = p_{am}(1 - \delta) \tag{A3}$$

The instantaneous pressure is a non-harmonic function that has a minimum at $\theta = \pi - \Theta$ and a maximum at $\theta = 2\pi - \Theta$.

The function $f(\delta)$ is defined in the interval $0 < \delta < 1$ by the following equation:

$$f(\delta) = \pi \frac{\sqrt{1-\delta^2} - (1-\delta^2)}{\delta} \tag{A4}$$

It is noted that some engines with a high degree of development have $f(\delta)$ values away from the maximum value of the function, which is equal to 0.943 for $\delta = 0.786$.

From the equations of $W_0/(p_{am}V_{sw})$ listed in Table A1, it is easy to identify the work of each piston for each engine configuration, which is an advantage of this type of formulation. Thus, the equation for the alpha-type engine has two terms of different sign, consistent with the work done on each of the pistons, whereas there is only one summand for the beta- and gamma-type engines, because the work realized by the displacer piston is null. The reader should note that $\sin\Theta$ is positive for an alpha-type engine, whereas it is negative for the beta- and gamma-type engines.

Walker [35] proposed an equivalent formulation for the Schmidt model of the alpha-type engine, according to which the indicated work can be calculated from the following equation:

$$W_0 = \pi\, p_m V_{sw}\, (1-\tau)\, \kappa\, \frac{1-\sqrt{1-\delta^2}}{\delta} \sin\Theta_W \tag{A5}$$

which can be re-written as follows,

$$\zeta_0 = f(\delta)\,(1-\tau)\,\kappa\,\sin\Theta_W \tag{A6}$$

where:

$$\Theta_W = \tan^{-1}\left[\frac{\kappa \sin\alpha_W}{\tau + \kappa\cos\alpha_W}\right] \tag{A7}$$

The equations in Table A1 can be converted to Walker's formulation by considering that the mean cycle pressure and the arithmetic mean pressure satisfy the following relation:

$$p_m = \oint p\,\mathrm{d}\theta = p_{am}\sqrt{1-\delta^2} \tag{A8}$$

and that Walker assumes a different reference for the crank angle, i.e.:

$$\theta_W = \pi - \theta - \alpha \tag{A9}$$

$$\alpha_W = -\alpha \tag{A10}$$

$$\Theta_W = \Theta - \alpha \tag{A11}$$

Table A1 Schmidt's model equations for the basic Stirling engine configurations.

Alpha-type engine	Beta-type engine (with maximum overlapping)	Gamma CEC-type engine
$v_E = \frac{V_E}{2}[1-\cos(\theta+\alpha)]$		
$v_C = \frac{V_C}{2}[1-\cos\theta]$	$v_C = \frac{V_E}{2}[1+\cos(\theta+\alpha)] + \frac{V_C}{2}[1-\cos\theta] - V_{MO}$ $V_{MO} = \frac{V_E}{2}\left[1+\kappa-\sqrt{1-2\kappa\cos\alpha+\kappa^2}\right]$	$v_C = \frac{V_E}{2}[1+\cos(\theta+\alpha)] + \frac{V_C}{2}[1-\cos\theta]$
$\frac{p}{p_{am}} = \frac{1-\delta^2}{1-\delta\cos(\theta+\Theta)}$		
$\frac{W_0}{p_{am}V_{sw}} = f(\delta)\kappa[\sin(\alpha-\Theta) - \kappa\sin\Theta]$	$\frac{W_0}{p_{am}V_{sw}} = f(\delta)\left[-\kappa^2\sin\Theta\right]$	
$\delta = \frac{\sqrt{\tau^2+2\kappa\tau\cos\alpha+\kappa^2}}{\tau+\kappa+2S}$	$\delta = \frac{\sqrt{(1-\tau)^2-2\kappa(1-\tau)\cos\alpha+\kappa^2}}{\tau+\sqrt{1-2\kappa\cos\alpha+\kappa^2}+2S}$	$\delta = \frac{\sqrt{(1-\tau)^2-2\kappa(1-\tau)\cos\alpha+\kappa^2}}{\tau+\kappa+2S+1}$
$\Theta = \tan^{-1}\left[\frac{\tau\sin\alpha}{\tau\cos\alpha+\kappa}\right]$	$\Theta = \tan^{-1}\left[\frac{(1-\tau)\sin\alpha}{(1-\tau)\cos\alpha-\kappa}\right]$	

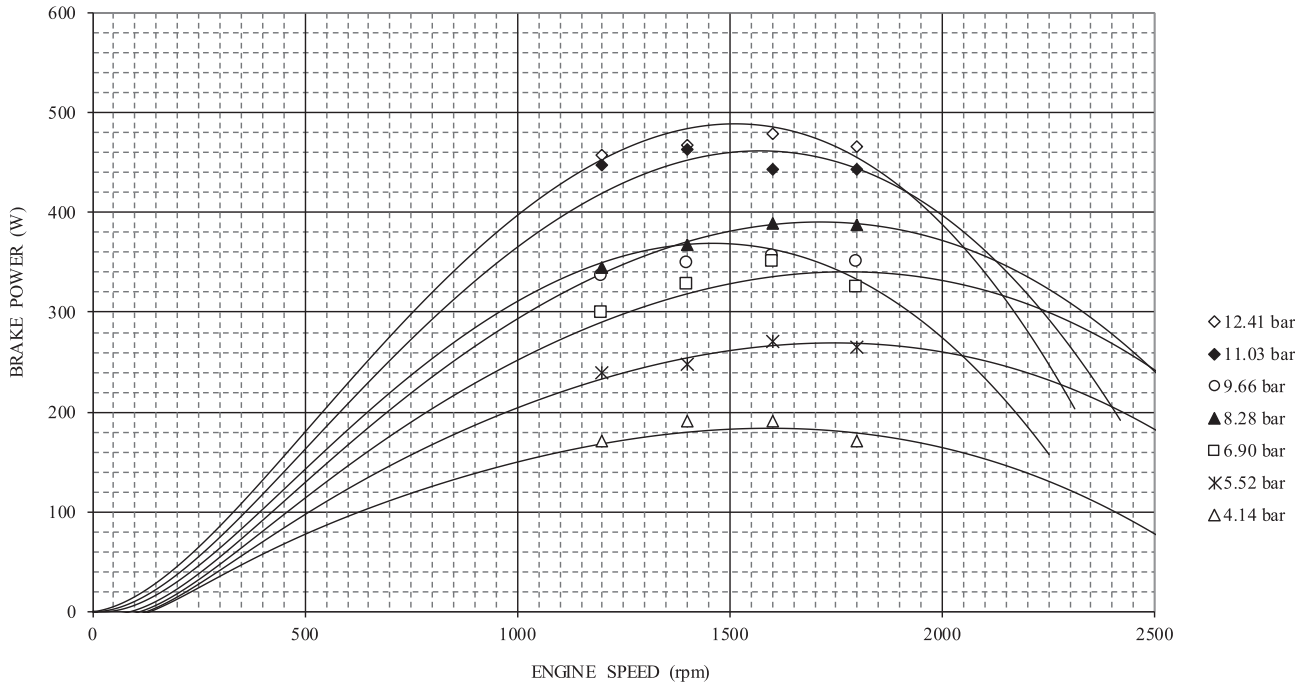

Fig. B1 Experimental data and brake power predictions for $T_{wE} = 900°C$.

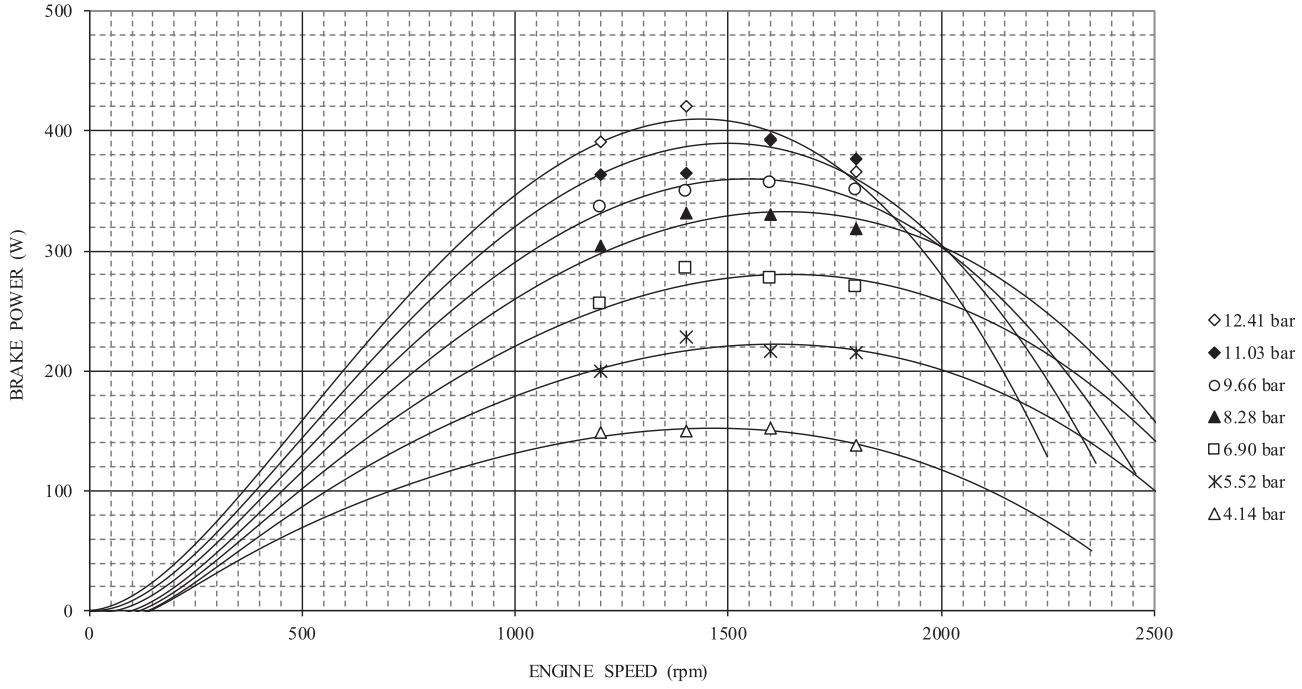

Fig. B2 Experimental data and brake power predictions for $T_{wE} = 800°C$.

Appendix B. Comparisons between experimental values and predictions from indirect characterization of the Philips M102C engine.

See Figs. B1-B4.

Appendix C. Temperature influence on mechanical power losses for the Philips M102C engine.

See Table C1.

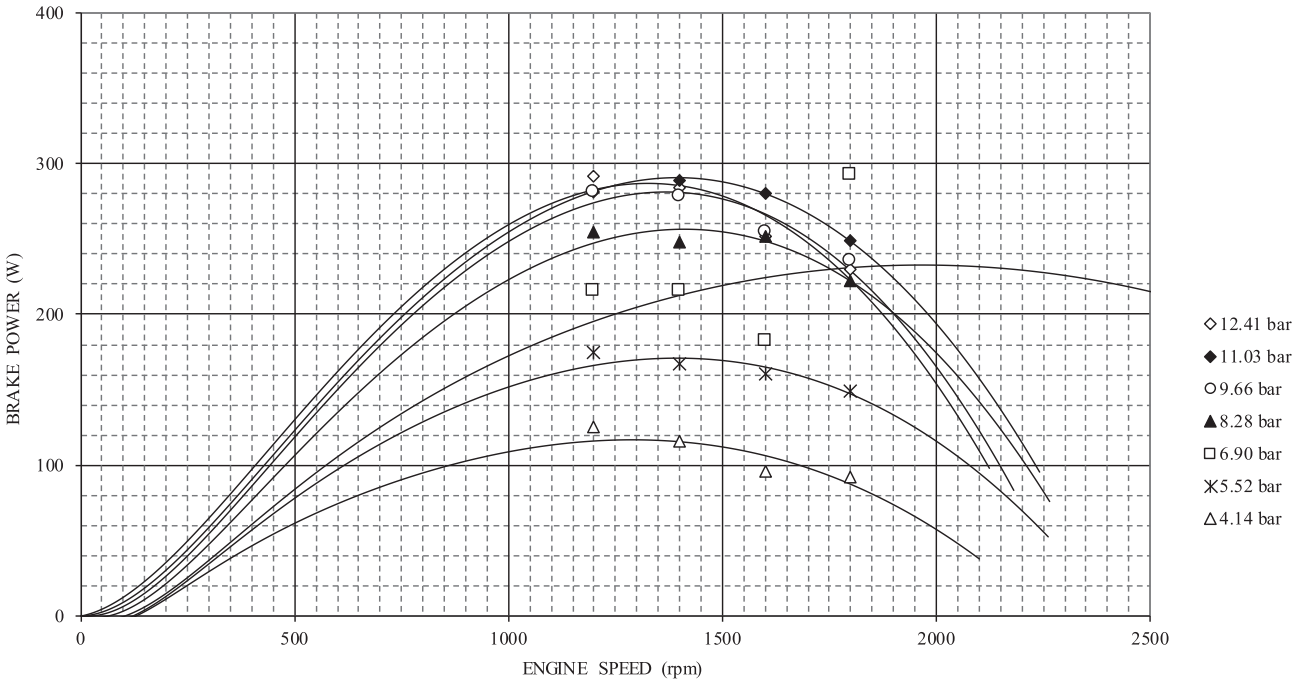

Fig. B3 Experimental data and brake power predictions for $T_{wE} = 700°C$.

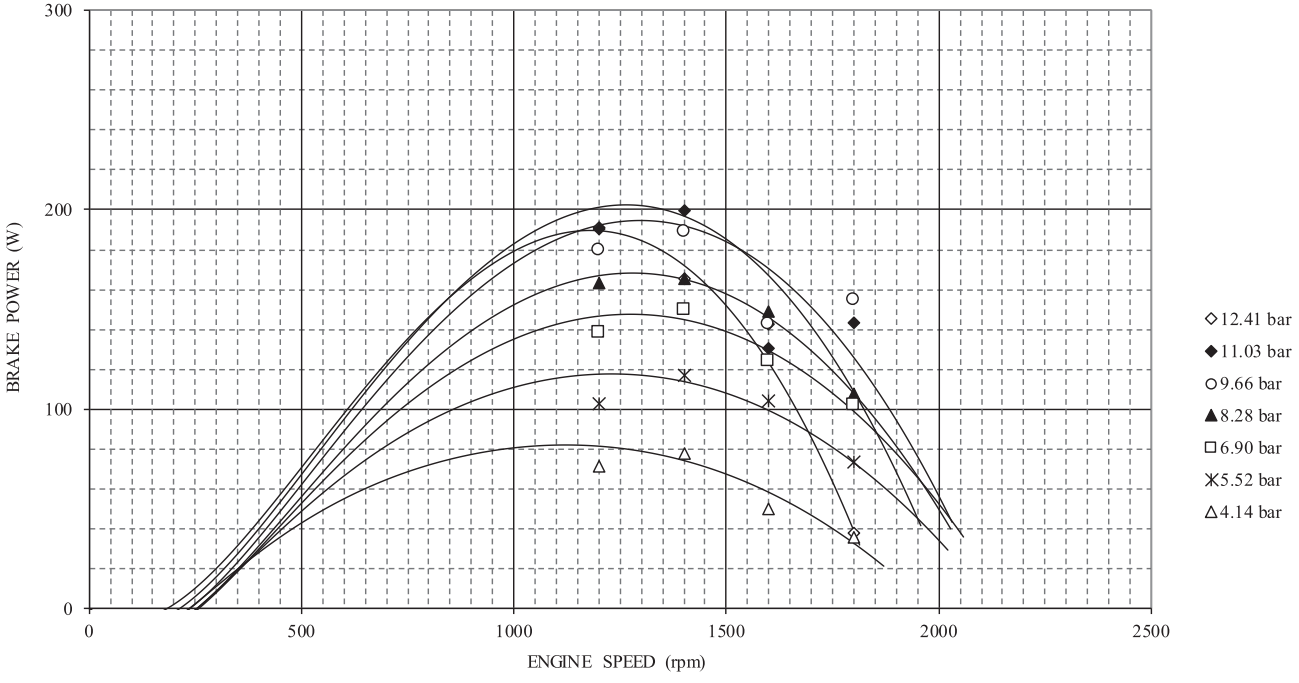

Fig. B4 Experimental data and brake power predictions for $T_{wE} = 600°C$.

Table C1 Comparisons of the values of $\zeta_{B,\max}$ and $N^*_{MA,\max}$ derived from applying equations (22), (24), and (25), and the values obtained if equation (23) is applied to all the series.

τ	N_p	$\zeta_{B,\max}$ [eq.(22)]	$\zeta_{B,\max}$ [eq.(23)]	relative error in $\zeta_{B,\max}$	$N^*_{MA,\max}$ [eq.(22)]	$N^*_{MA,\max}$ [eq.(23)]	relative error in $N^*_{MA,\max}$
0.2839	8.09E + 06	0.2432	0.2357	3.1%	0.00328	0.00336	2.5%
	7.19E + 06	0.2491	0.2411	3.2%	0.00340	0.00350	3.0%
	6.30E + 06	0.2448	0.2414	1.4%	0.00316	0.00319	1.0%
	5.40E + 06	0.2578	0.2479	3.8%	0.00370	0.00389	5.1%
	4.50E + 06	0.2602	0.2499	3.9%	0.00384	0.00406	5.6%
	3.60E + 06	0.2608	0.2509	3.8%	0.00378	0.00398	5.3%
	2.70E + 06	0.2614	0.2516	3.8%	0.00345	0.00358	3.9%
τ	N_p	$\zeta_{B,max}$ [eq.(24)]	$\zeta_{B,max}$ [eq.(23)]	relative error in $\zeta_{B,\max}$	$N^*_{MA,max}$ [eq.(24)]	$N^*_{MA,max}$ [eq.(23)]	relative error in $N^*_{MA,\max}$
0.3422	8.09E + 06	0.1633	0.1607	1.6%	0.00287	0.00290	1.0%
	7.19E + 06	0.1766	0.1759	0.4%	0.00302	0.00303	0.3%
	6.30E + 06	0.1990	0.1977	0.6%	0.00296	0.00298	0.5%
	5.40E + 06	0.2054	0.2048	0.3%	0.00306	0.00306	0.3%
	4.50E + 06	0.1602	0.1594	0.5%	0.00426	0.00422	0.9%
	3.60E + 06	0.2078	0.2078	0.0%	0.00301	0.00302	0.1%
	2.70E + 06	0.2040	0.2041	0.0%	0.00279	0.00279	0.1%
τ	N_p	$\zeta_{B,\max}$ [eq.(25)]	$\zeta_{B,\max}$ [eq.(23)]	relative error in $\zeta_{B,\max}$	$N^*_{MA,\max}$ [eq.(25)]	$N^*_{MA,\max}$ [eq.(23)]	relative error in $N^*_{MA,\max}$
0.3814	8.09E + 06	0.1214	0.1336	10.1%	0.00255	0.00244	4.4%
	7.19E + 06	0.1356	0.1205	11.1%	0.00274	0.00272	0.8%
	6.30E + 06	0.1448	0.1516	4.7%	0.00281	0.00272	3.3%
	5.40E + 06	0.1484	0.1530	3.1%	0.00277	0.00268	3.2%
	4.50E + 06	0.1570	0.1593	1.4%	0.00276	0.00269	2.3%
	3.60E + 06	0.1623	0.1521	6.3%	0.00266	0.00264	0.8%
	2.70E + 06	0.1652	0.1587	4.0%	0.00243	0.00238	2.0%

References

[1] G. Walker, E.R. Bingham, Low-capacity cryogenic refrigeration, Oxford University Press, New York, 1994.

[2] A. Depetro, G. Gamble, K. Moinuddin, Fire safety risk analysis of conventional submarines, Appl. Sci. 11 (2021) 2631.

[3] T. Mancini, P. Heller, B. Butler, B. Osborn, W. Schiel, V. Goldberg, R. Buck, R. Diver, C. Andraka, J. Moreno, Dish-Stirling Systems: an overview of Development and Status, J. Solar Energy Eng. 125 (2003) 135–151.

[4] T. Li, D.W. Tang, Z. Li, J. Du, T. Zhou, Y. Jia, Development and test of a Stirling engine driven by waste gases for the micro-CHP system, Appl. Thermal Eng. 33–34 (2012) 119–123.

[5] K. Wang, S.R. Sanders, S. Dubey, F.H. Choo, F. Duan, Stirling cycle engines for recovering low and moderate temperature heat: a review, Renew. Sustainable Energy Rev. 62 (2016) 89–108.

[6] C. Ulloa, P. Eguía, J.L. Miguez, J. Porteiro, J.M. Pousada-Carballo, A. Cacabelos, Feasibility of using a Stirling engine-based micro-CHP to provide heat and electricity to a recreational sailing boat in different European ports, Appl. Thermal Eng. 59 (2013) 414–424.

[7] M. Renzi, C. Brandoni, Study and application of a regenerative Stirling cogeneration device based on biomass combustion, Appl. Thermal Eng. 67 (2014) 341–351.

[8] P. Balcombe, D. Rigby, A. Azapagic, Environmental impacts of microgeneration: integrating solar PV, Stirling engine CHP and battery storage, Appl. Energy 139 (2015) 245–259.

[9] H. Al Moussawi, F. Fardoun, H. Louahlia-Gualous, Review of tri-generation technologies: Design evaluation, optimization, decision-making, and selection approach, Energy Convers. Manag. 120 (2016) 157–196.

[10] M. Mehrpooya, S. Sayyad, M.J. Zonouz, Energy, exergy and sensitivity analyses of a hybrid combined cooling, heating and power (CCHP) plant with molten carbonate fuel cell (MCFC) and Stirling engine, J. Cleaner Production 148 (2017) 283–294.

[11] M.H. Ahmadi, M.-A. Ahmadi, F. Pourfayaz, Thermal models for analysis of performance of Stirling engine: a review, Ren. Sust. Energy Reviews 68 (2017) 168–184.

[12] M. Babaelahi, H. Sayyaadi, A new thermal model based on polytropic numerical simulation of Stirling engines, Appl. Energy 141 (2015) 143–159.

[13] T. Finkelstein, Generalized thermodynamic analysis of Stirling engines, SAE Technical Paper 600222 (1960), https://doi.org/10.4271/600222.

[14] A. Organ, Intimate thermodynamic design of the Stirling engine gas circuit without the computer, Proc. Inst. Mech. Eng. C J. Mech. Eng. Sci. 205 (1991) 421–430.

[15] A. Organ, Thermodynamics and gas dynamics of the stirling cycle machine, Cambridge University Press, Cambridge, 1992.

[16] J.I. Prieto, Discussion on intimate thermodynamic design of the Stirling engine gas circuit without the computer, Proc. Inst. Mech. Eng. C J. Mech. Eng. Sci. 206 (1992) 219–220.

[17] J.R. Olson, G.W. Swift, Similitude in thermoacoustics, J. Acoust. Soc. Am. 95–3 (1994) 1405–1412.

[18] J.I. Prieto, R. Díaz, Isothermal simulation with decoupled losses for kinematic Stirling engine design, JSME Int. J. 36 (4) (1993) 697–1610.

[19] J.I. Prieto, J. Fano, R. Díaz, M.A. González, Application of discriminated dimensional analysis to the kinematic Stirling engine, Proc. Inst. Mech. Eng. C J. Mech. Eng. Sci. 208 (1994) 347–353.

[20] J.I. Prieto, M.A. González, C. González, J. Fano, A new equation representing the performance of kinematic Stirling engines, Proc. Inst. Mech. Eng. C J. Mech. Eng. Sci. 214 (2000) 449–464.
[21] J.I. Prieto, A.B. Stefanofskiy, Dimensional analysis of leakage and mechanical power losses of kinematic Stirling engines, Proc. Inst. Mech. Eng. C J. Mech. Eng. Sci. 217 (2003) 917–934.
[22] F. Formosa, L.G. Frèchete, Scaling laws for free piston Stirling engine design: benefits and challenges of miniaturization, Energy 57 (2013) 796–808.
[23] F. Sala, C.M. Invernizzi, D. García, M.A. González, J.I. Prieto, Preliminary design criteria of Stirling engines taking into account real gas effects, Appl. Thermal Eng. 89 (2015) 978–989.
[24] A.J. Organ, The Regenerator and the Stirling Engine, Mech. Eng. Publications, London, 1997.
[25] J.I. Prieto, M.A. González, C. González, J Fano, Notes on the scaling process of Stirling machines. In: Proceedings of the 7th International Stirling Conference on Stirling Cycle Machines, Tokyo, JP; 1995: 259–64.
[26] J.I. Prieto, J. Fano, C. González, M.A. González, R. Díaz, Preliminary design of the kinematic Stirling engine using dynamic similarity and quasi-static simulation, Proc. Inst. Mech. Eng. C J. Mech. Eng. Sci. 211 (1997) 229–238.
[27] J.I. Prieto, Discussion on analysis of the working process and mechanical losses in a stirling engine for a solar power unit, J. Solar Energy Eng. (Trans. ASME) 122 (2000) 207–208.
[28] D. García, J.I. Prieto, A non-tubular Stirling engine heater for a micro solar power unit, Renew. Energy 46 (2012) 127–136.
[29] D. García, M.J. Suárez, E. Blanco, J.I. Prieto, Experimental correlations and CFD model of a non-tubular heater for a Stirling solar engine micro-cogeneration unit, Appl. Thermal Eng. 153 (2019) 715–725.
[30] B. Kongtragool, S. Wongwises, Investigation on power output of the gamma-configuration low temperature differential Stirling engines, Ren. Energy 30 (2005) 465–476.
[31] A. J. Organ, Stirling Cycle Engines: Inner working and design; John Wiley & Sons, UK, 2014.
[32] J. Araoz, P. Platell, S. Larsson-Mastonstråle, Design analysis and control of the V2-6 Stirling engine, In: Proceedings of the18th International Stirling Engine Conference and Exhibition, Tainan, Taiwan; 2018.
[33] J.I. Prieto, Discussion on performance of stirling engines (arranging method of experimental results and performance prediction), JSME Int. J. B. 46 (1) (2003) 214–218.
[34] J.I. Prieto, Performance Characteristics and Preliminary Design Criteria of Stirling Engines. Hydrogen and Other Technologies Vol. 11, 2015, in: J.N. Govil, R. Prasad, S. Sivakumar, U.C. Sharma (Eds.), Energy Science & Technology (12 vol.), Studium Press LLC, Houston, TX, USA, 2015, pp. 439–480.
[35] G. Walker, Stirling engines, Clarendon Press, Oxford, 1980.
[36] D. García, M.A. González, J.I. Prieto, S. Herrero, S. López, I. Mesonero, C. Villasante, Characterization of the power and efficiency of Stirling engine subsystems, Appl. Energy 121 (2014) 51–63.
[37] S. Cho, S. Choi, C. Bae, An experimental measurement of lubrication behaviour of piston rings in a spark ignition engine, Jap. Soc. Mech. Engrs Int. J. (B) 45 (2) (2002) 373–378.
[38] I. Mesonero, S. López, F. García-Granados, F.J. Jiménez-Espadafor, D. García, J.I. Prieto, Indirect characterisation of indicated power in Stirling engines through brake power measurements, Appl. Thermal Eng. 100 (2016) 961–971.
[39] S. Alfarawi, R. Al-Dadah, S. Mahmoud, Enhanced thermodynamic modelling of a gamma-type Stirling engine, Appl. Thermal Eng. 106 (2016) 1380–1390.
[40] J. Bert, D. Chrenko, T. Sophy, L. LeMoyne, F. Sirot, Simulation, experimental validation and kinematic optimization of a Stirling engine using air and helium, Energy 78 (2014) 701–712.
[41] H. Hachem, R. Gheith, F. Aloui, S. Ben-Nasrallah, Numerical characterization of a γ-Stirling engine considering losses and interaction between functioning parameters, Energy Convers. Manag. 96 (2015) 532–543.
[42] I. Rodríguez, D. García, J.A. Celis, J.I. Prieto, Preliminary tests of trigeneration by means of biomass and Stirling engines, In: 7th International Congress of Energy and Environment Engineering and Management (CIIEM7), ScienceKNOW Conferences, Las Palmas, SP, 2017.
[43] C.M. Hargreaves, The Philips Stirling Engine, Elsevier Science Publishers, Amsterdam, 1991.